Correcting for water vapor diffusion in air bag samples for isotope composition analysis: cases studies with drone-collected samples

Di Wang[1,2,3*], Camille Risi[2], Lide Tian[1], Di Yang[1], Gabriel J. Bowen[4], Siteng Fan[2,5], Yang Su[6] , Hongxi Pang[7], Laurent Z.X Li[2]

[1] *Institute of International Rivers and Eco-security, Yunnan University, Yunnan Key Laboratory of International Rivers and Transboundary Eco–security, Kunming 650500, Yunnan, China*

[2] *Laboratoire de Météorologie Dynamique, IPSL, CNRS, Sorbonne Université, Campus Pierre et Marie Curie, Paris 75005, France*

[3] *Laboratoire Atmosphères, Observations Spatiales, IPSL, CNRS, UVSQ, Sorbonne Université, Guyancourt 78280, France*

[4] *Department of Geology and Geophysics, University of Utah, Salt Lake City, Utah 84108, USA*

[5] *Department of Earth and Space Sciences, Southern University of Science and Technology, Shenzhen 518055, China*

[6] *Département d'Informatique, École normale supérieure – PSL, 45 Rue d'Ulm, 75005 Paris, France*

[7] *Key Laboratory of Coast and Island Development of Ministry of Education, School of Geography and Ocean Science, Nanjing University, Nanjing 210023, China*

*Corresponding author: di.wang@latmos.ipsl.fr

删除[di wang]: di.wang@lmd.ipsl.fr

Abstract

Mass spectrometry and laser spectroscopy, have been widely employed for precise water vapor isotope measurements. Nevertheless, these techniques are limited by logistical challenges in fieldwork, consequently constraining the temporal and spatial resolution of measurements. Specifically, water vapor isotope measurements are primarily limited to near-surface levels, while measurements in the free troposphere are notably scarce. Portable sampling devices, such as air bags and glass bottles, have therefore become necessary alternatives for collecting, storing, and transporting gaseous samples in diverse environments prior to analysis with less portable instruments. In drone-based high-altitude vapor sampling, air bags are preferred for their lighter weight and greater flexibility compared to glass bottles. Nevertheless, they present specific challenges, such as potential sample contamination and isotopic fractionation during storage, primarily due to the inherent permeability of air bags. Here, we developed a theoretical model for water vapor diffusion through the sampling bag surface, with parameters calibrated through laboratory experiments. This model enables the reconstruction of the initial isotopic composition of sampled vapor based on measurements obtained within the bag and from the surrounding environment. This diffusion model underwent rigorous validation through experiments conducted under varying humidity and isotopic composition differences between the inside and outside of the air bag, confirming its reliability. We applied this correction method to air samples collected at various pressures up to the upper troposphere using an air bag-mounted drone that we developed, thereby estimating the initial isotopic composition and uncertainty based on our observations. The corrected observations closely match the Picarro in-suit observations and IASI satellite retrievals. Our correction method significantly enhances the reliability and applicability of water vapor isotope observations conducted using drones equipped with air bags. This approach leverages the strengths of drone-based air bag sampling while mitigating its limitations, thus facilitating the convenient collection of isotopic data throughout the troposphere.

删除[di wang]: Traditional methodologies, such as m

删除[di wang]: associated with processes aloft connecting tropospheric water vapor to surface precipitation

删除[di wang]: diverse conditions

删除[di wang]: direct

删除[di wang]: data

1 Introduction

Water vapor isotopes provide unique insights into the transport, mixing, and phase changes of water in the environment, which are crucial for improving understanding of the climate system, hydrological cycle, atmospheric dynamics, and paleoclimate proxies. Water isotopes have also been applied in climate modeling, weather prediction, and water resource management (Bowen et al., 2019; Galewsky et al., 2016; Gat, 1996; West et al., 2009).

Water isotope analysis has traditionally relied on mass spectrometry, which, while accurate (Ghosh and Brand, 2003; Muccio and Jackson, 2009), demands labor-intensive preparation and lacks portability (West et al., 2010). Methods like cryogenic trapping effectively collect water vapor (Grootes and Stuiver, 1997; Michener and Lajtha, 2008; Steen-Larsen et al., 2011; Yu et al., 2015), but they require long sampling periods, limiting observation scope and timing. Over the past three decades, laser spectroscopy methods such as Cavity Ring-Down Spectroscopy (CRDS)(Hodges and Lisak, 2006) and Off-Axis Integrated Cavity Output Spectroscopy (OA-ICOS) (Johnson et al., 2011) have emerged, delivering a best-in-class combination of speed, high precision, and continuous measurements even in challenging environments such as high altitudes or arid regions with low water vapor content. Advances in these instruments have significantly expanded the field of water isotope research. However, their heavy instrumentation, substantial power requirements, and limited mobility restrict their usability in certain situations, particularly for aerial water vapor isotope measurements, which require lightweight and flexible sampling approaches. As a result, the collection and storage of physical samples are still necessary, increasing the demand for more convenient and efficient sample acquisition methods. Air bags and glass bottles have been practical solutions for collecting, storing, and transporting gaseous samples from various settings (Jiménez-Rodríguez et al., 2019; Rozmiarek et al., 2021).

Given that air bags can reduce the weight of sampling equipment and increase sampling flexibility, there is considerable interest in using them for vapor sample collection. This is particularly advantageous for small equipment like drones, where minimizing payload weight is essential for sampling at high altitudes or over long distances. This selection also makes it easier to transport samples and reduces the risk of breakage. However, concerns have arisen regarding the suitability of various sampling materials for storing these samples, primarily due to potential water diffusion through container walls. Diffusion issues are commonly observed in sampling bags during water vapor isotope analysis and have persisted as a longstanding challenge in the field (Herbstritt et al., 2023; Jiménez-Rodríguez et al., 2019). In previous studies, this issue is particularly concerning in the Direct Vapor Equilibrium Laser Spectroscopy (DVE-LS) method, which has been widely used to rapidly collect and measure water isotopes in evaporation-prone soil, rock, or plant samples. The DVE-LS method simplifies preparation and increases sample throughput by directly analyzing the vapor phase, thus eliminating the need for extensive physical extractions (Gralher et al., 2021; Hendry et al., 2015; Millar et al., 2018; Sprenger et al., 2015; Wassenaar et al., 2008). However, water vapor molecules may exchange between the air inside the bag and the external ambient air during sample storage. Water vapor molecules typically diffuse from areas of high humidity to drier areas. In this process, heavier isotopologues (e.g., $H_2{}^{18}O$ and HDO) move more slowly

删除[di wang]:

删除[di wang]: isotopes

than lighter isotopologues (e.g., $H_2{}^{16}O$) due to their greater mass, resulting in preferential diffusion of lighter isotopes. This differential diffusion, can alter the original isotopic composition of the collected air samples. Moreover, differential diffusion can also occur due to gradients in isotopic composition.

To mitigate these issues, materials with lower permeability are suggested for water vapor isotope measurements (Herbstritt et al., 2023). Further research and development are still necessary. This may involve exploring alternative materials for more impermeable sampling bags, improving sealing methods to better isolate sampled air, and developing sampling techniques less susceptible to diffusion. Resolving these issues is essential for ensuring the reliability of water vapor isotope measurements using air bags and for accurately understanding atmospheric and hydrological processes.

In light of the ongoing development and further refinement of these techniques and the associated cost constraints, we developed a diffusion model with parameters calibrated through laboratory experiments. This model is capable of assessing the permeability of the air bags and correcting the obtained isotope measurements to the initial pre-diffusion values based on the humidity, isotope values inside and outside the bag, and the sample storage time. This diffusion model was validated through experiments under varying humidity and isotopic composition differences between the inside and outside of the air bag, confirming its reliability. Furthermore, we also applied this diffusion method to air samples collected at different altitudes using a drone-based atmospheric vapor sampling device we developed, to estimate the initial isotope composition and uncertainty. The primary objective of this drone-based field campaign is to obtain atmospheric water vapor isotope data along vertical profiles in the troposphere, providing higher temporal and spatial resolution than satellite observations. The corrected near-surface drone-based measurements using our diffusion model show consistency with direct, in-situ surface-level measurements using the Picarro analyzer. Similarly, at two mid-tropospheric levels, the corrected drone measurements align with IASI satellite observations of water vapor isotopic composition, further confirming the model's theoretical and practical reliability in applications.

删除[di wang]: isotopes

删除[di wang]: selective

删除[di wang]: known as fractionation,

删除[di wang]: values

删除[di wang]: diverse conditions

删除[di wang]: data for

删除[di wang]: Picarro direct

删除[di wang]: observations and satellite data

2 Theoretical basis of diffusion model

2.1 Diffusion model description

Storing vapor samples in air bags prior to isotope measurement may alter the isotopic composition of the water vapor. The main reason is the diffusion of water molecules between the interior and exterior of the air bags, primarily due to the permeability of the bag materials. We present a mathematical model for the diffusion and fractionation of isotopes across the surface of the sampling bag. In this model, we assume the ambient vapor flux entering the air bag changes the internal humidity and vapor isotopc composition, influenced by the different humidity and water isotopc composition inside and outside the bag (Fig.1).

The flux of water into the bag, F (in $kg/m^2/s$), is expressed as:

$$F = k * (q_e - q(t)) \quad (1)$$

where q(t) represents the variation of humidity inside the air bag over time (in kg/kg), q_e

删除[di wang]: e values

删除[di wang]: e values

删除[di wang]: Note that we use isotope ratios (R) in the following equations for mathematical convenience and conciseness, but present isotope values δ in figures in subsequent sections for visualization purposes.

删除[di wang]: toward

denotes the environmental humidity (in kg/kg).

Similarly, the flux of isotopologue, F_i, either $H_2{}^{18}O$ or HDO, moving into the bag can be described as:

$$F_i = k_i * (R_e * q_e - R(t) * q(t)) \quad (2)$$

In this equation, k_i represents the conductance specific to each isotopologue (in $kg/m^2/s$), R_e denotes the isotopic ratio in the environment, and R(t) is the variation of isotopic ratio within the air bag with time. Notably, the fractionation coefficient can be denoted as:

$$\alpha = \frac{k}{k_i} \quad (3)$$

The validity of Equation (1) and (2) relies on the assumptions that internal and external pressures remain equal to atmospheric pressure, ensuring no pressure gradient across the bag membrane, that the internal vapor is well-mixed, and that the exchange rate follows a first-order process. Additionally, if the temperature remains constant, k and k_i are assumed to be constant.Assuming that diffusion through the bag is the primary transport mechanism, and neglecting adsorption, the temporal change in humidity can be modeled by the following differential equation:

$$\frac{d(q(t)*M)}{dt} = F * A \quad (4)$$

where A represents the exchange area (surface area of the air bag), and M is the air mass inside the bag.

Assuming that M is constant, which is reasonable given that the total mass variation due to water vapor flux is at most 1%, this equation simplifies to:

$$\frac{dq(t)}{dt} = \frac{F*A}{M} = \frac{k*A}{M} * (q_e - q(t)) \quad (5)$$

Here, we define the water vapor conductance , as follows, it describes the rate at which water vapor exchanges across the bag membrane:

$$\lambda = \frac{k*A}{M} \quad (6)$$

Similarly, the temporal change in isotopic ratio can be modeled by the following differential equation:

$$\frac{d(R(t)*q(t)*M)}{dt} = M * (q(t) * \frac{dR(t)}{dt} + R(t) * \frac{dq(t)}{dt})$$

$$= F_i * A = k_i * (R_e * q_e - R(t) * q(t)) * A \quad (7)$$

This equation can be simplified as:

$$\frac{dR(t)}{dt} = \frac{ki*(R_e*q_e - R(t)*q(t))*A/M - R(t)*\frac{dq(t)}{dt}}{q(t)}$$

$$= \frac{\frac{k*A}{M*\alpha}*(R_e*q_e - R(t)*q(t)) - R(t)*\frac{k*A}{M}*(q_e - q(t))}{q(t)}$$

$$= \frac{\frac{\lambda}{\alpha}*(R_e*q_e - R(t)*q(t)) - R(t)*\lambda*(q_e - q(t))}{q(t)}$$

$$= \frac{\lambda}{\alpha} * (R_e - R(t)) \pm \frac{\lambda}{q(t)} * (q_e - q(t)) * (\frac{R_e}{\alpha} - R(t)) \quad (8)$$

删除[di wang]: , and k is a constant (in $kg/m^2/s$)
删除[di wang]: toward
删除[di wang]: a constant
删除[di wang]: by
删除[di wang]: .
删除[di wang]:
删除[di wang]: The
删除[di wang]: 3
删除[di wang]: If
删除[di wang]: 4
删除[di wang]: diffusion coefficient of humidity
删除[di wang]: ,
删除[di wang]: , as λ.
删除[di wang]: 5
设置格式[di wang]: 法语(法国)
设置格式[di wang]: 法语(法国)
设置格式[di wang]: 法语(法国)
设置格式[di wang]: 法语(法国)
设置格式[di wang]: 法语(法国)
删除[di wang]:
设置格式[di wang]: 法语(法国)
删除[di wang]: 6

If q_e is stable (the environment is treated as an infinite reservoir), and that k and A are constant, the differential equation for humidity (Eq. 5) can be analytically solved :

$$q_e - q(t) = (q_e - q_0) * e^{(-\frac{k*A}{M}*t)} = (q_e - q_0) * e^{(-\lambda*t)} \quad (9)$$

where q_0 is the initial humidity at t = 0. This equation can also be expressed in terms of natural logarithms as:

$$\ln(q_e - q(t)) = \ln(q_e - q_0) - \lambda * t \quad (10)$$

Consequently, the slope of ln(q_e - q(t)) against time is λ.

For the isotopic ratio, the analytical solution is only feasible when the initial humidity equals the environmental humidity ($q_0 = q_e$) :

$$\frac{dR(t)}{dt} = \frac{k*A}{M*\alpha} * (R_e - R(t)) \quad (11)$$

Assuming that R_e, q_e, k, α and A are constant:

Thus, $$R_e - R(t) = (R_e - R_0) * e^{(-\frac{k*A}{M*\alpha}*t)} \quad (12)$$

where R_0 denotes the initial isotopic ratio at t = 0. Again, taking the natural logarithm, we obtain:

$$\ln(R_e - R(t)) = \ln(R_e - R_0) - \frac{\lambda}{\alpha} * t \quad (13)$$

This equation demonstrates that the slope of ln(R_e-R(t)) against time is the water vapor isotopic conductance $\frac{\lambda}{\alpha}$. Knowing λ, we can deduce the isotopic fractionation coefficient due to fractionation caused by mass flow through bags, α, for each isotope.

However, when the environmental humidity differs from the initial humidity inside the air bag, a numerical solution is required to solve the differential equation for R (Eq. 8).

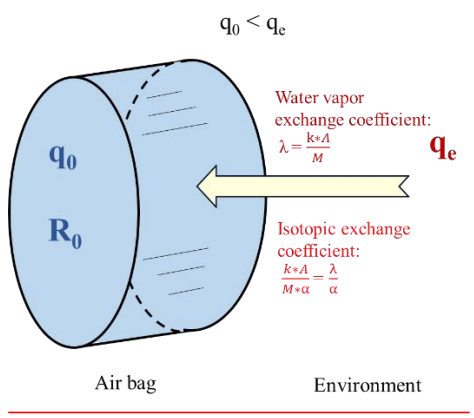

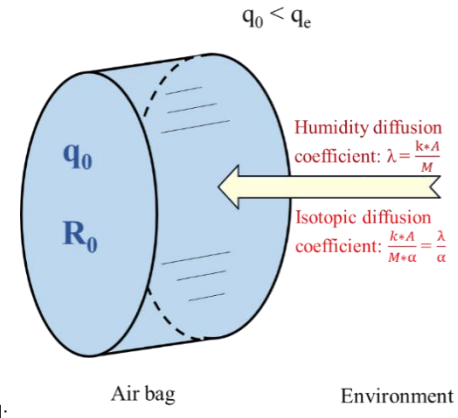

Figure 1 Schematic illustrating the diffusion model. q_0 *represents the initial humidity in the air bag at t = 0,* q_e *denotes the environmental humidity,* R_0 *indicates the initial isotopic ratio in the air bag at t = 0,* R_e *represents the isotopic ratio in the environment, k is water vapor conductance, A denotes the exchange area (surface area of the bag), and M is the mass of air within the bag, and* α *denotes the isotopic fractionation coefficient.*

删除[di wang]: T
删除[di wang]: 4
删除[di wang]: 7
删除[di wang]: 8
删除[di wang]: 9
删除[di wang]: 10
删除[di wang]: 11
删除[di wang]: diffusion coefficient of isotopic ratio
删除[di wang]: 6
删除[di wang]: *a constant*

2.2 Reconstructing initial water vapor isotopic compositions

The isotopic composition of the air bag water vapor undergoes an exponential evolution over time (Eq. 12). This method of applying exponential evolution equations to reconstruct isotopic compositions has been used in environmental forensics to investigate shifts in water isotopes due to metabolic changes, environmental conditions, or diet (Ayliffe et al., 2004; Cerling et al., 2006). Similarly, in climatology, this method helps retrieving initial isotopic composition from samples such as ice cores or tree rings, affected by evaporation, precipitation, and temperature fluctuations, facilitating historical climate reconstruction (Brienen et al., 2016). Here we apply a similar method, and apply the analytical solution of Equation 8 using data from experiments in which the condition that q_0 equals q_e is met to determine the equation parameters.

The constants (λ, $\alpha_{^{18}O}$, $\alpha_{^{2}H}$) can be determined through laboratory experiments and Eqs. 10 and 13 (see Subsection 3.2 and 4.1). If we know the initial values within the air bag (q_0, $R_{^{18}O_0}$, $R_{^{2}H_0}$), the ambient values (q_e, $R_{^{18}O_e}$, $R_{^{2}H_e}$), and the storage time ($T_{storage}$) of the sampling bag, we are able to simulate the variations in humidity and isotopic ratios inside the air bag according to Eqs. 5 and 8. Similarly, if we know $T_{storage}$, the humidity and isotopic composition at time $t = T_{storage}$ ($q_{(T\_storage)}$, $R_{^{18}O_{(T\_storage)}}$, $R_{^{2}H_{(T\_storage)}}$) in the air bag, and the ambient values, we can deduce the initial values in the air bag at t = 0 by back-calculating. The equation used for reconstructing the initial isotope ratio (R_0) is:

$$R_0 = R_{measured} = \int_0^{T_{storage}} \frac{dR(t)}{dt} dt$$

$$= R_{measured} = \int_0^{T_{storage}} \left(\frac{\lambda}{\alpha} * \left(R_e - R(t)\right) \pm \frac{\lambda}{q(t)} * \left(q_e - q(t)\right) * \left(\frac{R_e}{\alpha} - R(t)\right)\right) dt \quad (14)$$

where R_0 represents the initial isotopic ratio to be reconstructed, $R_{measured}$ is the observed isotopic ratio after $T_{storage}$, and $\frac{dR(t)}{dt}$ is defined in Eq. 8.

This approach allows us to correct for diffusion-induced isotopic shifts and reconstruct the original vapor composition.

For mathematical clarity and consistency, isotopic ratios (R) are used in the equations presented in previous sections. Replacing R with δ-values would only shift the physical basis without affecting the mathematical validity of the equations or the estimation of α, as the standard ratio cancels out. For clearer visualization, δ-values are used for numerical applications and in the subsequent figures and tables.

删除[di wang]: 10
删除[di wang]: values
删除[di wang]: 6
删除[Administrator]: δ
删除[Administrator]: δ
删除[di wang]: uation
删除[di wang]: 8
删除[di wang]: 11
删除[di wang]: δ
删除[di wang]: δ
删除[di wang]: δ
删除[di wang]: δ
设置格式[di wang]: 下标
删除[di wang]: uation
删除[di wang]: 4
删除[di wang]: 6
删除[di wang]: the storage time
设置格式[di wang]: 下标
删除[di wang]: values
设置格式[di wang]: 下标
设置格式[di wang]: 下标
删除[di wang]: t
删除[di wang]: δ
设置格式[di wang]: 下标
删除[di wang]: t
删除[di wang]: δ
设置格式[di wang]: 下标
删除[di wang]: t
设置格式[di wang]: 下标
设置格式[di wang]: 下标
设置格式[di wang]: 缩进: 左侧: 0 毫米, 左 0 字符, 首
设置格式[di wang]: 字体: （默认）Times New Roman
设置格式[di wang]: 法语(法国)
设置格式[di wang]: 缩进: 左 3.5 字符, 悬挂缩进: 2 字符

3 Methods and data

删除[di wang]:

3.1 Air bag isotope measurements

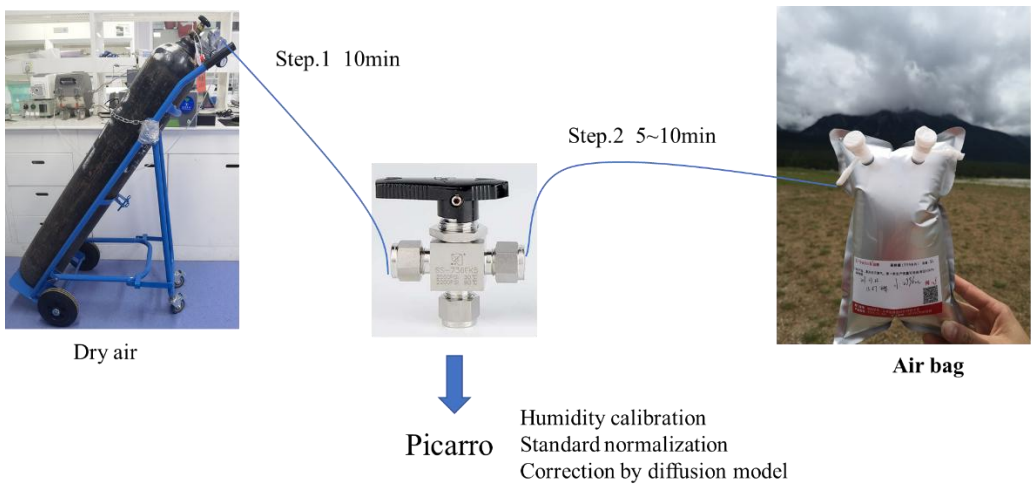

Figure 2 Setup for isotope measurements using air bags with a Picarro atmospheric water vapor isotope analyzer.

In this study, we used 0.5 L and 4L Teflon air bags produced by Dalian Hede Technologies Co., Ltd to collect and store vapor, and measured the vapor isotopes using a Picarro 2130i water isotope analyzer. Based on our testing and the airflow rate set for the Picarro analyzer, the 0.5 L and 4 L bags provided sufficient sample volume for approximately 17 minutes and 130 minutes of analysis, respectively.

删除[di wang]: 25

删除[di wang]: 200

Figure 2 illustrates the setup for measuring vapor isotopes in air bags. In this system, the air inlet of the Picarro isotope analyzer was connected to a three-way valve through Teflon or stainless steel tubing. The other two ports of the three-way valve were attached to the outlet valve of the air bag and a dry air cylinder, respectively. Sample storage and measurement were conducted in a temperature-regulated room to maintain constant temperature conditions for the air bags and tubing.

In the measurement procedure, we first activated the dry air cylinder and adjusted the pressure reducing valve to 2 psi (pounds of force per square inch), within the Picarro water isotope analyzer's recommended range of 2–4 psi for carrier gas. The instrument's built-in flow regulation maintains a gas flow rate of 30–50 mL/min, ensuring stable sample delivery. We then opened the valve channel connecting the dry air cylinder to the three-way valve, allowing dry air to flow into the isotope analyzer and flush all air pathways for 10 minutes. Subsequently, we closed the dry air channel, opened the air bag outlet valve, and the corresponding valve channel on the three-way valve. This allowed water vapor in the air bags to be analyzed at a constant temperature in the Picarro analyzer, a process lasting between 5 and 10 minutes. Upon completion, we switched the valve to measure dry air. By repeatedly measuring isotopic composition for replicate samples—air samples collected simultaneously under the same conditions—we achieved greater accuracy in the water vapor measurements.

删除[di wang]: set the flow rate at

删除[di wang]: e values

删除[di wang]: parallel samples

删除[di wang]: ,

To correct isotope measurement bias caused by the instrument's sensitivity to different

删除[di wang]: can

water vapor concentrations (JingfengLiu et al., 2014; Schmidt et al., 2010), we used the built-in Standard Delivery Module (SDM) of the Picarro 2130i water vapor isotope analyzer to generate a 500–25,000 ppm water vapor gradient for isotope measurements. We selected 20,000 ppm as a reference humidity level, as this corresponds to the optimal accuracy range of the Picarro analyzer (JingfengLiu et al., 2014; Schmidt et al., 2010). All the measured vapor isotope data were normalized to the VSMOW-SLAP scale using two distinct laboratory reference waters with known isotopic composition. Before conducting daily measurements, we adjusted the quantity of the injected liquid standard to align with the humidity of the external vapor measurements.

3.2 Laboratory permeability experiments

To evaluate the variations of the diffusion of water molecules between the interior and exterior of the air bags, we conducted the following experiments (Table S1), as detailed below:

3.2.1 Experiment No. 1: Quantification of $\lambda_{surface}$

To quantify the water vapor conductance at the surface, $\lambda_{surface}$, using Eq.10, we filled the empty and clean air bags with dry air and measured humidity variations using a Picarro analyzer at intervals of 1 minute, 2, 4, 6, 8, and 10 hours following the measurement method described in Subsection 3.1. Measurements were conducted using 0.5L and 4L air bags, with repetitions on both identical and different air bags of the same dimensions (refer to the experiment times in Table 1 and results in Fig.3a). We measured $\lambda_{surface}$ (=k*A/M) under near-surface pressure and temperature we set in a controlled chamber. While k may vary with temperature and pressure, these effects were assumed negligible within the condition of our study. Results will be shown in Subsection 4.1.

3.2.2 Experiment No. 2: Quantification of α

To investigate isotope variation patterns and improve measurement accuracy during storage in the air bag to quantify the isotopic fractionation coefficient, α, using Eq.13, initial values significantly different from ambient conditions were selected. Empty, clean air bags were first filled with dry air, f, then sealed by closing the bag valve. To maintain a closed system while injecting reference water, a dedicated injection septum was installed on the valve. After reopening the valve, a fixed amount of laboratory reference liquid water with known isotopic composition was injected into the dry air-filled bag using a 10 μL injection needle. isotopic composition In Experiment No. 2, we ensured that q_0 was approximately equal to q_e. To ensure $q_0 = q_e$, the environmental vapor concentration was first measured, followed by the calculation and experimental determination of the water volume to be injected into the air bag. Water vapor concentration and isotope variations within the air bags were then measured using a Picarro analyzer at intervals of 5 minutes, 2, 4, 6, 8, and 10 hours. Results will be shown in Subsection 4.1. To ensure data consistency and reliability, we

删除[di wang]: the humidity-dependent isotope bias

删除[di wang]: we applied a calibration function by measuring vapor isotopes with gradient vapor concentrations set using a standard delivery module (SDM)

删除[di wang]: set

删除[di wang]: a reference level of

删除[di wang]: for vapor humidity in our analysis

删除[di wang]: considering

删除[di wang]: at this specific humidity level

删除[di wang]: isotopic values

删除[Administrator]: *Table 1 Summary of experiments: diffusion parameter quantification, model validation and differences in experimental methods. $\lambda_{surface}$ denotes the diffusion coefficient of humidity at the surface, α_δ refers to the fractionation coefficient of isotopes, q_0 represents the*

删除[di wang]: diffusion coefficient of humidity

删除[di wang]: uation

删除[di wang]: 8

删除[di wang]: 2

删除[di wang]:

设置格式[di wang]: 图案: 清除(白色)

删除[Administrator]: **_δ**

删除[di wang]: Equation

删除[di wang]: 11

删除[di wang]: ollowed by the injection of a fixed amount of water with known isotopic values

删除[di wang]: ,

删除[di wang]: ensuring

repeated these measurements multiple times using air bags of both the same and different sizes, including 0.5L and 4L bags. For the 0.5L air bags, a separate bag was prepared for each time interval, and water vapor concentration and isotopic compositions were measured once to ensure that the parameter M remained stable without being affected by repeated measurements. However, manual injection of reference water with known isotopic composition introduced some variability, causing minor variations in initial values across all bags. This is evident in Figs. 5, 6, and S2, where q_0 = 1/2 q_e data exhibit slight fluctuations due to the use of separate bags for each time interval. To address this, we repeated the experiment with 4L air bags, measuring the same air bag at different time intervals, which ensured consistent initial conditions at t=0 but allowed M to change over time. When air bags differ only in size, the parameter λ associated with A and M varies, while the isotopic fractionation coefficient α is theoretically constant. Both approaches could contribute to uncertainties in the mismatches between the model and experimental results. Therefore, we incorporated the results from both the 0.5 L and 4 L experiments into our uncertainty estimation of these mismatches, as detailed in Subsections 3.2.3 and 3.4.2.

删除[di wang]: isotopic values

删除[di wang]: , making it difficult to ensure identical initial conditions across all bags.

删除[di wang]:

3.2.3 Experiment No. 3: Diffusion model validation

To validate the diffusion model under diverse conditions and evaluate its uncertainties, we repeated Experiment No. 2, but injected different amounts of water with known isotopic composition to achieve a range of humidities from approximately 1/8 * q_e to q_e. Using the method described in Experiment No. 2, we injected 6 to 50 μL of reference water into a 4L air bag filled with dry air to achieve the desired humidity range. Additionally, we isotopic compositionrepeated the experiment using two reference waters with distinct isotopic compositions, specifically $\delta^{18}O$ = -58.07‰, $\delta^{2}H$ = -447.41‰ and $\delta^{18}O$ = -29.84‰, $\delta^{2}H$ = -222.84‰. To assess extended-duration variations, we also lengthened the time interval to 24 hours.

Once the parameters of the diffusion model have been obtained through Experiments No. 1 and 2, we used this model to simulate the variations in water vapor humidity and isotopic composition inside the air bag over time for Experiments No. 2 and 3 (refer to Section 2). When simulating these experiments using the diffusion model, we used measurements taken after a 5-minute delay as the initial condition to ensure that it represented complete evaporation of the injected water. We then simulated the temporal variations in humidity and vapor isotopes within the air bag using a 5-minute time step using Eqs.5 and 8, separately. The resulting outputs (hereafter referred to as 'the diffusion model simulations') will be shown in Subsection 4.2 and code are available as supplementary material.

删除[di wang]: isotopic values

删除[di wang]: used water with different isotopic values

删除[di wang]: to replicate the experiment.

设置格式[di wang]: 字体: （中文）等线

删除[Administrator]: can

删除[di wang]: e values

删除[di wang]: Results

3.3 Drone-mounted systems and field campaign

We designed and built a collection module for fixed-height sampling, incorporating diaphragm vacuum pumps, a rudder mounted on the drone, and a control module linked to a remote operating system. When the drone reaches a specified altitude, we remotely activate the designated air pump to inflate a specific air bag. Once sampling is complete, the pump is deactivated, and the drone ascends to the next target altitude, where the corresponding air

删除[di wang]: constructed

删除[di wang]: at predetermined altitudes

删除[di wang]: using

删除[di wang]: air pumps and

删除[di wang]: along with

pump inflates another air bag. This process was repeated until all predetermined samples were collected. Self-sealing diaphragm vacuum pumps were used to transfer air into the sampling bags. Once the pump ceased operation, it remained sealed from the external environment, preventing unintended air ingress. Additionally, due to the flexible nature of the air bags, internal and external pressures remained balanced. As air pressure increases during the drone's descent after collection. To further prevent the loss of collected air samples, a one-way valve was installed to block backflow. Additionally, the one-way valve helps prevent large droplets from entering the air bag during the collection process.

The sampling module was mounted on our specially designed high-altitude drones and deployed during a field campaign conducted from June 25, 2020, to October 17, 2020, in the pristine forests of Mountain Laojun, Lijiang, on the southeastern edge of the Tibetan Plateau and the northwestern of the Yunnan-Guizhou Plateau, China. We collected water vapor samples every 500 meters, starting from near the surface along the vertical profile. To optimize sampling across different altitude ranges, we deployed UAVs designed for varying flight altitudes. Generally, the UAV operating at lower altitudes collected samples at seven heights from 4,000 to 7,000 meters in a single flight. The mid-altitude UAV collected samples at four heights from 7,500 to 9,000 meters in one flight, while the high-altitude UAV collected samples at four heights from 9,500 to 11,000 meters in two flights. Each flight took approximately 20~30 minutes. In case of any disruptions during sampling, we repeated the process until a complete vertical profile was obtained. At the beginning of the experiment, we also collected replicate samples at each height to ensure data consistency.

By integrating high-altitude drone sampling with subsequent water vapor isotope analysis using the Picarro analyzer , at the surface, we obtained vapor isotopic profiles up to an altitude of 11 km. Unlike conventional methods, such as cryogenic vapor sampling, this approach requires much less sample volume and allows for timely measurements. Additionally, compared to large aircraft, airships, and balloon-based observations, this method is relatively low-cost and supports more flexible and long-term observations.

3.4 Application of diffusion model to vertical profiles

3.4.1 Estimating the air mass in the bag

λ is defined as k*A/M and depends on the air mass M in the bag. In drone-based vertical sampling, M varies with altitude due to pressure changes, requiring an estimate of λ for different altitudes (λ_{alt}). However, since λ is an intrinsic property of the bag material, its apparent variation reflects uncertainties in estimating collected M, which depend on atmospheric pressure (P), sampling time, and pump efficiency (ε):

$$M_{alt} = M_{surface} * \frac{P_{surface}}{P_{alt}} * \frac{\text{Sampling time}_{alt}}{\text{Sampling time}_{surface}} * \varepsilon \quad (15)$$

where M_{alt} is the air mass collected at a different altitude and $M_{surface}$ represents the air mass collected at the surface. At higher altitudes, where the air pressure (P_{alt}) is lower than at

删除[di wang]: However, as air pressure increases during the drone's descent after collection, the air bags may deflate, potentially causing leakage of the collected air samples. To address this, we installed a one-way valve that permits only air entry into the bag, thus preventing backflow.

删除[di wang]: region

删除[di wang]: , throughout the period from June 25, 2020, to October 17, 2020

删除[di wang]: with in-situ

删除[di wang]: measurements

删除[di wang]: in-situ

删除[di wang]: For the vertical profile samples collected using drones, since λ (k*A/M) depends on M, and M acquired by the sampling bag varies due to different sampling altitudes with varying air pressure, λ consequently varies with altitude as well. However, it is difficult to experimentally estimate λ for different altitudes (λ_{alt}); instead, we estimated it from the variation of the collected M.

设置格式[di wang]: 下标

删除[di wang]:
At higher altitudes, where the air pressure (P_{alt}) is lower than at the surface ($P_{surface}$), less air will be pumped into the air bag. To compensate for this effect, a longer sampling time was used at higher altitudes (Sampling $time_{alt}$) than at the surface (Sampling $time_{surface}$) (Fig.A1). Therefore,

删除[di wang]: 12

the surface ($P_{\_surface}$), less air will be pumped into the air bag. To compensate for this effect, a longer sampling time was used to collect air at higher altitudes ($Sampling\ time_{\_alt}$) than at the surface ($Sampling\ time_{\_surface}$) (Fig.A1).

Given that $\lambda_{\_alt}$ is proportional to $M_{\_alt}$, we calculated it as:

$$\lambda_{\_alt} = \lambda_{\_surface} * \frac{P_{\_surface}}{P_{\_alt}} * \frac{Sampling\ time_{\_alt}}{Sampling\ time_{\_surface}} * \varepsilon \quad (16)$$

where $\lambda_{\_surface}$ is the λ quantified experimentally at the surface.

Since air pressure and sampling times were directly measured, the primary source of error for $M_{\_alt}$, and consequently $\lambda_{\_alt}$, arises from pump efficiency (ε), which may decrease over time and at lower pressures. Using the estimated $\lambda_{\_alt}$, the observed vertical isotope profiles were corrected based on Eq.14 from Section 2.2. The uncertainty estimation is discussed in Section 3.4.2..

3.4.2 The method of uncertainty estimation

Potential errors in correcting vertical profiles using the diffusion model include estimates of $\lambda_{\_surface}$, α, pump efficiency (ε), and mismatches between model and experiments (Table 1). We detail each below:

1) $\lambda_{\_surface}$ uncertainty: laboratory experiments provided upper and lower bounds on $\lambda_{\_surface}$ (Subsection 4.1). These were used for error estimation.

2) α uncertainty: the λ and λ/α were first estimated from several experiments, from which α was calculated. Their averaged values were used separately to parameterize the model. As highlighted in Subection 3.2.2, estimating λ/α (and subsequently calculating α) requires results from cases where q_0 equals q_e, minor variations in q_0 and fluctuations in q_e could introduce non-systematic discrepancies between the model and experimental results. Consequently, for analyzing the contribution of α to uncertainties, only αderived from experiments where the model closely matched the majority of experimental results were considered. Selection criteria for these experiments included minimal deviation between q_0 and q_e, minimal deviation between experimental data and simulations, and stable q_e, ensuring the reliability of the chosen α.

3) Pump efficiency (ε) uncertainty: The efficiency of the pump may decline over time or vary with atmospheric pressure, affecting the collected air mass M. To account for this, we applied a conservative uncertainty range of 0.75 to 1.25 relative to surface conditions, ensuring the full range of possible variations in $M_{\_alt}$ was considered.

4) Model-experiment mismatches: We compared model simulations with experimental data across 87 cases, calculating the average absolute discrepancy. These mismatches were included as an additional uncertainty component.

Total Uncertainty Calculation: The maximum discrepancy across all calibration results—using the full uncertainty range for $\lambda_{\_surface}$, α, and pump efficiency (ε)—was determined. The model-experiment mismatch was then added as an independent error component. The final uncertainty estimates, reported in Subsections 4.3 to 4.5, account for all potential error.

设置格式[di wang]: 下标
删除[di wang]: Therefore, the λ at a higher altitude ($\lambda_{\_alt}$)
删除[di wang]: 13
删除[di wang]: All sampling times were recorded during
删除[di wang]: sources of
删除[di wang]: correction process
删除[Administrator]: _δ
删除[di wang]: $\lambda_{\_alt}$
删除[di wang]: from
删除[di wang]: 2
删除[di wang]: For
设置格式[di wang]: 非上标/ 下标
删除[di wang]: ,
删除[di wang]: the uncertainty range was estimated through
删除[di wang]: by considering the minimum and maximu
删除[di wang]: . The results are presented in
删除[di wang]: For
删除[Administrator]: _δ
删除[di wang]: ,
删除[di wang]: average values of
删除[di wang]:
删除[di wang]: and then
删除[di wang]: can be
删除[di wang]: The results are presented in Subsection 4.
删除[di wang]: .
设置格式[di wang]: 下标
设置格式[di wang]: 下标
删除[di wang]: However, in these numerous experiments,
删除[di wang]: data.
删除[di wang]: values
删除[di wang]: values
删除[di wang]: values
删除[di wang]: Regarding the
设置格式[di wang]: 下标

Table 1 Uncertainties and estimation methods

Uncertainties	Number of experiments	Estimation method	Used value (min~max for error es
$\lambda_{surface}$	7 (0.5L bags); 6 (4L bags)	Obtained from lab experiments (max & min)	For 0.5L air bags: 0.031(0.0291~ For 4L air bags: 0.0255(0.0250~
α	4	Obtained from lab experiments	α_^{18}O is 1.0241, α_^{2}H is 1.0 (α_^{18}O is 1.0254, α_^{2}H is 1.05 α_^{18}O is 1.0264, α_δ^{2}H is 1.038
Pump efficiency (ε)	-	0.75~1.25 relative to surface conditions	0.75~1.25
Mismatches between model and experiments	87	Average of all difference between experimental data and simulations	0.5 ‰ for δ^{18}O, 4.1 ‰ for δ^{2}H, 2 d-excess

3.5 Satellite isotope data IASI

Several satellite missions have contributed to water vapor isotope observations, including the Tropospheric Emission Spectrometer (TES) onboard Aura (2004–2018) (Worden et al., 2006), the Scanning Imaging Absorption Spectrometer for Atmospheric Cartography (SCIAMACHY) onboard Envisat (2002–2012), the Atmospheric Infrared Sounder (AIRS) onboard Aqua (since 2002) (Worden et al., 2019), and the Tropospheric Monitoring Instrument (TROPOMI) onboard Sentinel 5 Precursor (since 2017) (Schneider et al., 2022). In this study, we use the MUSICA retrievals from the Infrared Atmospheric Sounding Interferometer (IASI) onboard METOP due to its broad spatiotemporal coverage, vertical profiling capability, and the availability and accessibility of its dataset (Diekmann et al., 2021). It has a horizontal footprint of approximately 12 km at nadir (directly below the satellite), increasing with the angle of observation. This configuration ensures nearly global coverage twice daily.

In this study, we compared our observed vapor δ^{2}H profiles up to the upper troposphere with satellite observations. Due to the intermittent availability of IASI data at any given location, we limited our comparison of observational results across various altitudes at our study site to days when IASI data were available. Satellite measurements, particularly for vertical profiles of water vapor isotopes, are inherently different from direct sampling, they represent a vertical average over layers determined by the averaging kernels (Rodgers and Connor, 2003; Worden et al., 2006). Therefore, their comparability with ground-based or drone-based observations, which provide high-resolution local data, is limited. The MUSICA retrievals from the IASI satellite instrument provides water vapor isotope data at three altitude levels: 1-3 km in the lower troposphere, 4-7 km in the mid-troposphere, and 8-12 km in the upper troposphere. Given that our study started at an altitude of 3856 m, we used the retrieved δ^{2}H data for the 4–7 km and 8–12 km levels. However, these measurements represent a

删除[di wang]: To evaluate the total error, we computed the maximum discrepancy between all calibration results, which used the uncertainty ranges of the first three potential sources mentioned above, and the corrected data employed. To this value, we added the fourth error source, which is the mismatch observed between the model and the experiments. The final uncertainties present in Subsections 4.3 and 4.5 represent the maximum error derived from all four error sources.

删除[di wang]: *2*

删除[di wang]: *Uncertainty*

删除[di wang]: *sources*

删除[di wang]: Uncertainty

删除[di wang]: sources

删除[Administrator]: δ

删除[Administrator]: δ

删除[Administrator]: _δ

删除[Administrator]: δ

删除[Administrator]: δ

删除[Administrator]: δ

删除[di wang]: ± ¼

删除[di wang]: Sampling time_alt

删除[di wang]: Recorded sampling time

删除[di wang]: Of the available instruments, the Infrared Atmospheric Sounding Interferometer (IASI) offers the best spatiotemporal coverage for δ^{2}H retrieval (Lacour et al., 2012; Lacour et al., 2018)

删除[di wang]: typically have limited vertical resolution. The IASI satellite instrument provides water vapor isotope

vertical average over layers determined by the averaging kernels (Rodgers and Connor, 2003; Worden et al., 2006). While using averaging kernels to smooth the observed profile could facilitate a more quantitative analysis, we simply averaged the observations for the corresponding altitudes. Consequently, the comparison remains mainly qualitative.

4 Results

4.1 Parameter estimates

The $\lambda_{surface}$ was determined through laboratory Experiment No. 1. Based on Eq. 10, the parameter λ_surface was estimated to be 0.0312 (uncertainty range: 0.0291 to 0.0317) for the 0.5 L air bags and 0.0255 (uncertainty range: 0.0250 to 0.0259) for the 4 L air bags (Fig. 3a, Table 1).

The isotopic fractionation coefficients, α, were determined through laboratory Experiment No. 2. From the averaged results of these measurements, using Eq. 13, the water vapor isotopic conductance, expressed as λ/α, was estimated to be 0.0249 for ^{18}O and 0.0244 for ^{2}H (Fig. 3b and c). Consequently, $\alpha_{^{18}O}$ was estimated to be 1.0241 (0.0255/0.0249), and $\alpha_{^{2}H}$ was estimated to be 1.0451 (0.0255/0.0244) (Fig. 3b and d). Two additional sets of fractionation coefficients, α, were obtained: $\alpha_{^{18}O}$ = 1.0254, $\alpha_{^{2}H}$ = 1.0506, and $\alpha_{^{18}O}$ = 1.0264, $\alpha_{^{2}H}$ = 1.0380 (Table 1).

The specific parameter values obtained in this study pertain to the Teflon air bags used in the aforementioned tests, conducted at an ambient temperature of 16°C. These values depend on bag material, temperature, and pressure, which should be considered when applying the model under different conditions. We also noted batch-to-batch variations among air bags from the same manufacturer. Besides, we apply these parameters measured under ground-level storage and measurement conditions, assuming negligible temperature and pressure effects on λ and α during the short (10–20 min) drone-based sampling period. Future work is needed to quantify these dependencies.

删除[di wang]: Equation
删除[di wang]: 8
删除[di wang]: 2
删除[di wang]: Equation
删除[di wang]: 11
删除[di wang]: diffusion coefficient of isotopic composition
删除[Administrator]: δ
删除[Administrator]: δ
删除[Administrator]: δ
删除[Administrator]: δ
删除[Administrator]: δ
删除[Administrator]: δ
删除[Administrator]: δ
删除[Administrator]: δ
删除[di wang]: 2
删除[di wang]:
删除[di wang]: These parameters determined were influenced by factors such as the type and material composition of the air bags and ambient temperature.
删除[di wang]: The acquired parameters specifically
删除[di wang]: ed

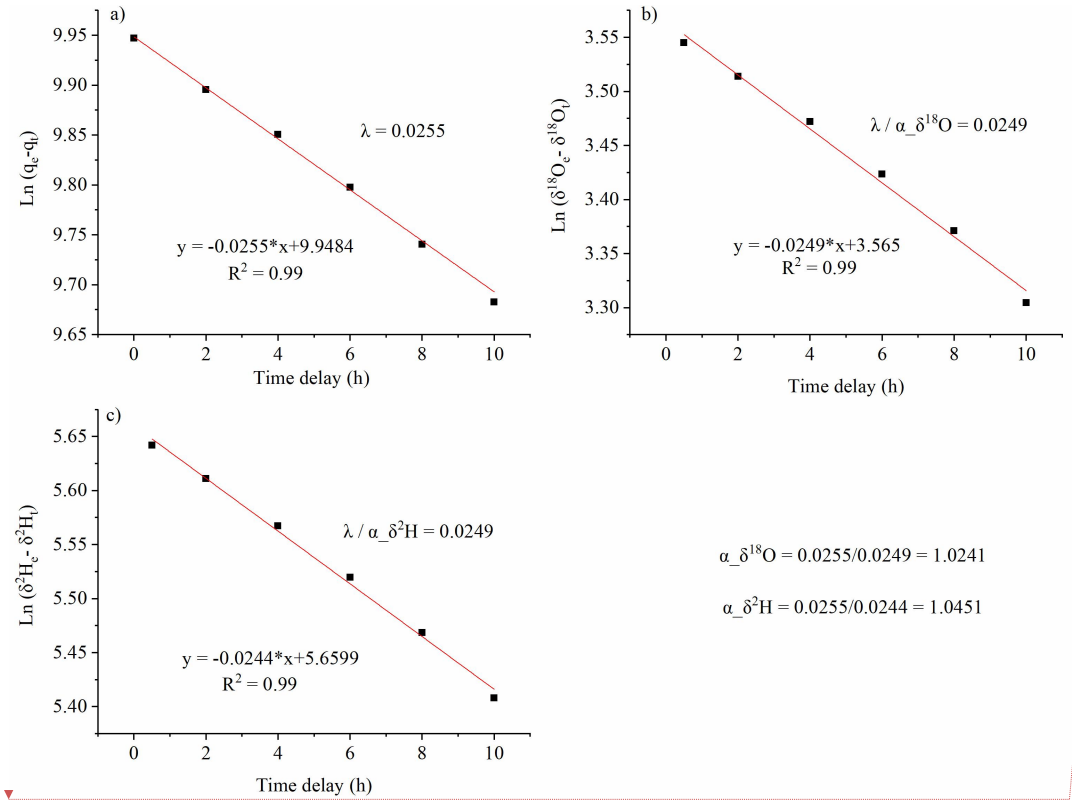

453

Figure 3 Determination of 3 parameters of the diffusion model : λ_surface (a) from Experiment No. 1, α_^{18}O// (b), and α_^{2}H (c) from Experiment No. 2.

删除[di wang]: These parameters determined were influenced by factors such as the type and material composition of the air bags and ambient temperature.We observed some differences between batches of air bags from the same manufacturer, which are worth noting. The primary objective of this study was to establish a methodology.

删除[Administrator]: δ

4.2 Diffusion model validation

4.2.1 General case

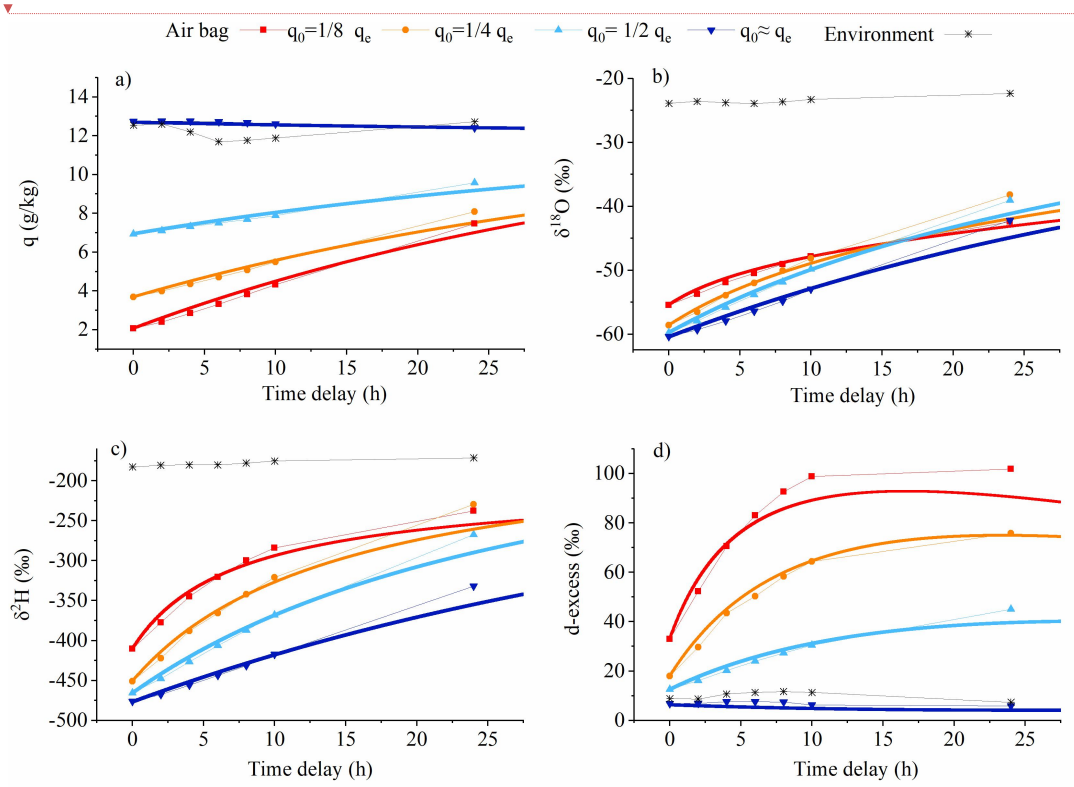

*Figure 4: Comparison of the variation within the air bag over time in laboratory permeability experiments (markers) and diffusion model simulations (lines) across a range of initial humidities at t = 0 (q_0), ranging from approximately 1/8 * q_e to q_e (q_e denotes the environmental humidity), under the condition that the water vapor isotopic composition in the air bag significantly differs from ambient values : a) humidity; b) $\delta^{18}O$; c) $\delta^{2}H$, d) d-excess.*

To validate the model, we used Experiment No.3 described in Subsection 3.2. The diffusion model simulations (lines in Figs. 4, 5, 6, and Fig. S2) are in close agreement with our experimental observations (markers in Figs. 4, 5, 6, and Fig. S2), showing consistency in humidity, $\delta^{18}O$, $\delta^{2}H$, and d-excess variations, with only minor deviations. Shorter storage times produce fewer deviations. When the humidity inside the air bag is lower than the ambient level, vapor from the environment enters the air bag, resulting in a gradual increase in humidity (Fig. 4a and Fig. S2). Meanwhile, because the water vapor isotopic composition in the air bag is significantly lower than the ambient values, $\delta^{18}O$ and $\delta^{2}H$ in the air bag gradually increase and toward ambient values as ambient moisture enters the bags over time (Fig. 4b and c). In contrast, the d-excess increase as the time delay progresses due to kinetic fractionation during moisture diffusion into the air bag (Fig. 4d), as detailed in the following Subsection 4.2.2.

删除[di wang]:

删除[di wang]: simulations from our

删除[di wang]: (Fig.4)

删除[di wang]: values

471 *We observed that some curves unexpectedly intersect, which can be understood by*
472 *analyzing Eq. (8). The first term* $(\frac{\lambda}{\alpha}(R_e - R_{(t)})$ *continuously drives* $R_{(t)}$ *towards* R_e*, while the*
473 *second term* $(\frac{\lambda}{q(t)}(q_e - q_{(t)})(\frac{Re}{\alpha} - R_{(t)})$ *modulates the rate of change. Initially, for simulations*
474 *with lower* q_0 *(e.g., the red and orange curves),* $q_e - q_{(t)}$ *is large, making the second term*
475 *significant and positive, thereby increasing* $R_{(t)}$ *more rapidly. However, as* $R_{(t)}$ *exceeds* R_e/α*,*
476 *the sign of this term reverses, slowing down the increase in* $R_{(t)}$ *compared to other curves. In*
477 *contrast, curves with higher initial* q_0 *(e.g., blue curve) experience a steadier growth and*
478 *eventually surpass the initially faster-growing curves, leading to the observed crossing.*

479 **4.2.2 Particular cases**

480

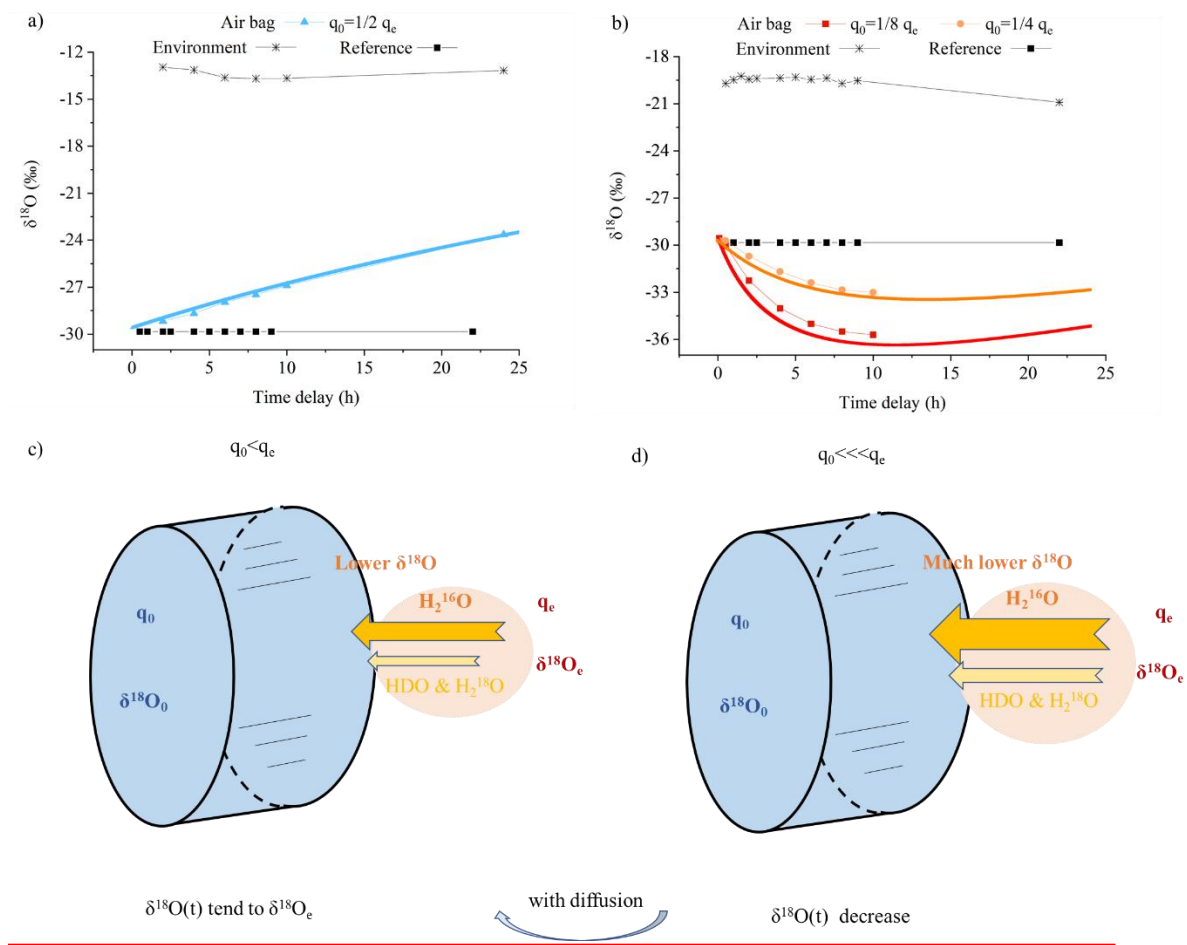

481 *Figure 5 (a-b) Variations of* $\delta^{18}O$ *under different conditions: (a) when both the differences between internal* ($\delta^{18}O_0$) *and external* ($\delta^{18}O_e$) $\delta^{18}O$ *as well as between internal* (q_0) *and external* (q_e) *humidity are not significant,* $\delta^{18}O$ *gradually increases toward equilibrium; (b) when* q_0 *is significantly lower than* q_e*, a stronger vapor influx causes enhanced kinetic fractionation, leading to a decrease in* $\delta^{18}O$*. (c-d) Corresponding schematics: (c) illustrates the mechanism for (a), where a weaker humidity gradient results in slower isotopic shifts, while (d) corresponds to (b), showing intensified fractionation with a larger gradient, with*

设置格式[di wang]: 字体: 11 磅
设置格式[di wang]: 字体: 11 磅
设置格式[di wang]: 字体: 11 磅
设置格式[di wang]: 字体: 11 磅
设置格式[di wang]: 字体: 11 磅
设置格式[di wang]: 字体: 11 磅
设置格式[di wang]: 字体: 11 磅
设置格式[di wang]: 字体: （中文）等线

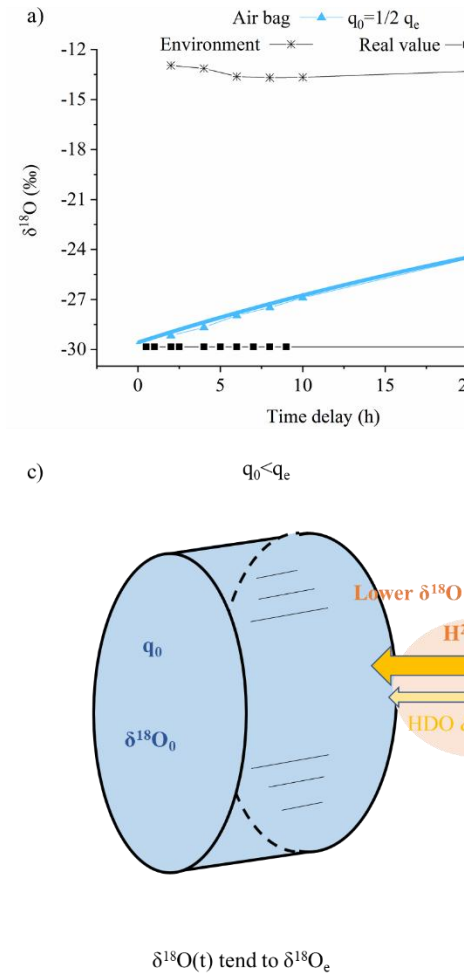

删除[di wang]:
删除[di wang]: *(a, b)*
删除[di wang]: *values*
删除[di wang]: *the difference between* $\delta^{18}O_0$ *and* $\delta^{18}O_e$ *is*
设置格式[di wang]: 非上标/ 下标
设置格式[di wang]: 非上标/ 下标
删除[di wang]: ,
删除[di wang]: *illustrations of the underlying mechanis*

arrows indicating vapor flux direction and fractionation intensity. $\delta^{18}O$ (t) is the variation of $\delta^{18}O$ within the air bag over time. In (a) and (b), the colored lines represent model simulations based on Eq.8, using parameterization from Experiments No. 1 and 2. Colored square markers show the corresponding experimental observations within the air bags. Black square markers indicate the initial values inside the air bag, which remain constant over time and serve as a reference for comparison (legend: Reference).

Due to isotopic kinetic fractionation, lighter $H_2{}^{16}O$ molecules preferentially diffuse into the air bag compared to heavier isotopologues such as $HD^{16}O$ and $H_2{}^{18}O$, resulting in a vapor flux with lower $\delta^{18}O$ relative to ambient vapor (Fig. 2). Moreover, variations within the air bag are driven by differences in water vapor content and isotopic ratios between its interior and exterior, as described in the diffusion model in Section 2. As shown in the initial experiment (Fig. 4b and c), when the internal $\delta^{18}O$ and δ^2H are significantly below the ambient values, the δ-values of the diffusing vapor, although lower than ambient, still exceeds the initial internal δ-values, leading to a gradual increase towards the ambient values; diffusion simply equilibrates the isotopic composition in the bag and the environment. When the disparity between internal and external $\delta^{18}O$ or δ^2H is not very substantial, and humidity differences are also minimal, the weaker diffusive gradient produces less net kinetic fractionation. This results in a small amount of vapor with lower $\delta^{18}O$ and δ^2H than the ambient moisture entering preferentially, but not falling below internal initial values, thereby still drives a progressive increase in the internal values towards ambient moisture (Fig. 5a and c). In contrast, with the same initial contrast between internal and ambient δ-values, that is, the disparity between internal and external $\delta^{18}O$ and δ^2H is less pronounced, but q_0 is much lower than q_e, there is a stronger net flux into the bag, and this flux fractionates more rapidly; much more vapor with significantly lower $\delta^{18}O$ and δ^2H than the ambient moisture (and lower values than the initial internal vapor) enters the air bags and dominates their isotopic composition, thereby reducing the internal δ-values (Fig.5b and d). The smaller the difference in humidity and isotopic composition between the inside and outside of the air bag, the slower and smaller the isotopic change in the vapor within the air bag (Fig. 5 and Fig. 6).

删除[Administrator]: first scenario in Figure

删除[Administrator]: :

删除[di wang]: values

删除[di wang]: Similarly, in the second scenario in Figure 5a and c, w

删除[Administrator]: and

删除[di wang]: values

删除[di wang]: values

删除[di wang]: ing

删除[di wang]: values

删除[Administrator]:

删除[Administrator]: as in the first scenario

删除[Administrator]: in the third scenario in Figure 5b and d

删除[di wang]: values

删除[di wang]: values

删除[Administrator]: As diffusion progresses, the difference in humidity and isotopic composition between the inside and outside of the air bag decreases, causing the third scenario to evolve into the second scenario.

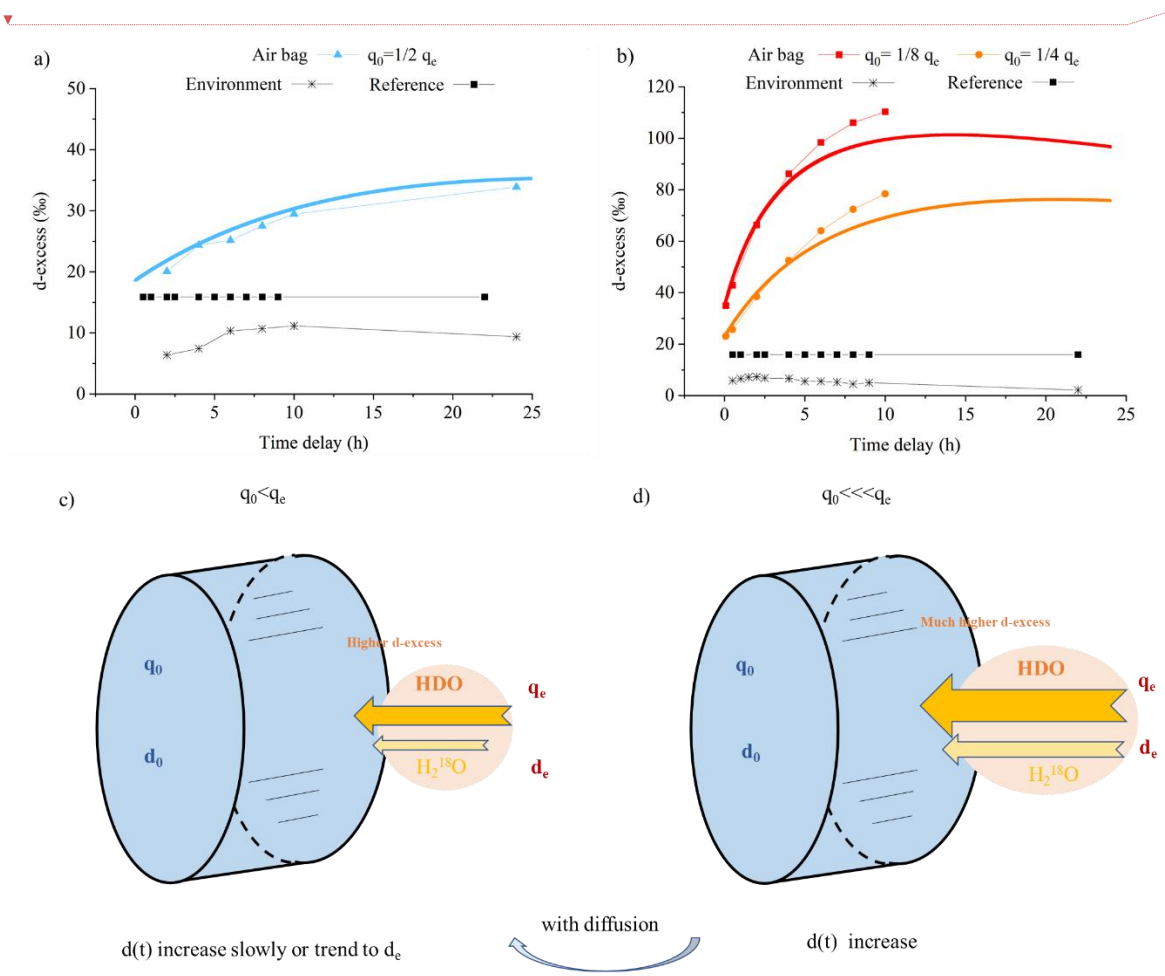

Figure 6 (a-b) Same as Fig.5, but showing the evolution of d-excess in cases: (a) when the difference between the humidity inside (q_0) and outside (q_e) the air bag is not significant, d-excess increases gradually; (b) when q_0 is significantly lower than q_e, a stronger vapor influx enhances kinetic fractionation, causing a more rapid d-excess increase. (c-d) Corresponding schematics: (c) illustrates the mechanism for (a), where a smaller humidity gradient results in slower isotopic shifts, while (d) corresponds to (b), showing intensified fractionation with a larger gradient. d_0 *indicates the initial d-excess at t = 0,* d_e *represents the d-excess in the environment. d(t) denotes the variation of d-excess within the air bag over time.*In addition, because HDO and $H_2{}^{18}O$ diffuse at similar rates the magnitude of the kinetic fractionation for D and ^{18}O is similar. However, since d-excess reflects deviations relative to the 8:1 fractionation ratio typical of equilibrium processes, the tendency is for kinetic fractionation during diffusion to contribute vapor with high d-excess and cause an increase in d-excess during air bag storage as water vapor is added to the bag (Fig. 6a and c). When the humidity difference between the inside and outside of the air bag increases, the d-excess of the incoming vapor flux increases as a result of more intensive kinetic fractionation. This leads to a faster increase in the vapor d-excess inside the air bag (Fig. 6b and d).

Regardless of the differences in water vapor humidity and isotopic compositions inside and outside the air bag, the diffusion model simulations closely match the experimental observations (Figs.5 and 6). Using the method described in Subsection 3.4.2, the average difference between all simulations and experimental data for each parameter represented the

删除[di wang]: d(t) increase slowly or trend to d_e

删除[di wang]: *E*

设置格式[di wang]: 字体: 11 磅

设置格式[di wang]: 字体: 11 磅

设置格式[di wang]: 字体: 11 磅

设置格式[di wang]: 字体: 11 磅, 非上标/ 下标

设置格式[di wang]: 字体: 11 磅

删除[di wang]: *(c-d) Corresponding schematic illustrations of the underlying mechanisms for (a) and (b)*

删除[di wang]: *value*

删除[di wang]:

删除[di wang]: value

删除[Administrator]: In all scenarios, r

model-experiment mismatch: 0.5 ‰ for $\delta^{18}O$, 4.1 ‰ for $\delta^{2}H$, and 2.9 ‰ for d-excess.

4.3 Raw and corrected vertical profiles

Here, we present a summary of drone-based observations from the field campaign at Mount Laojun, Lijiang, on the southeastern edge of the Tibetan Plateau and the northwestern of the Yunnan-Guizhou Plateau, China, conducted between June 25, 2020, and October 17, 2020.

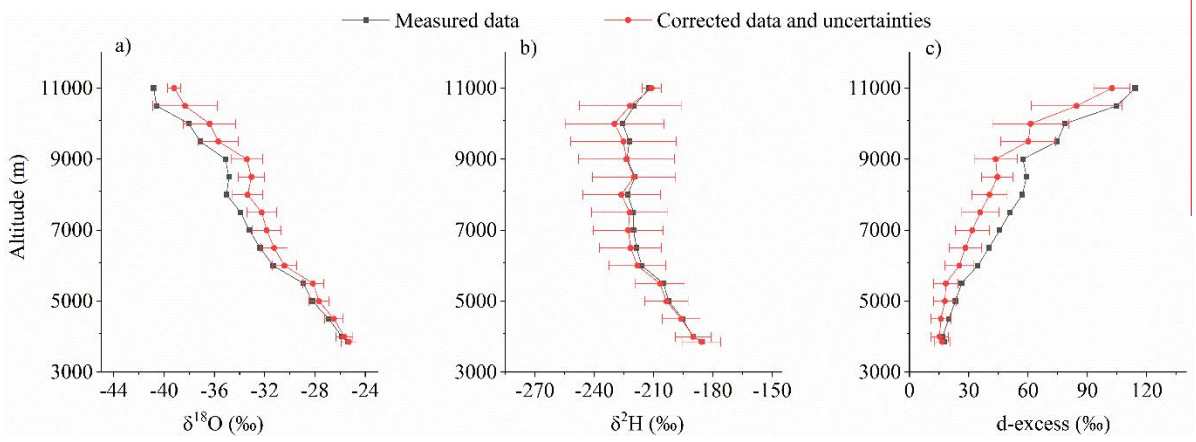

Figure 7 Comparison of vertical profiles for the mean values of all raw measurements and corrected data from June to October, and associated uncertainties for $\delta^{18}O$ (a), $\delta^{2}H$ (b) and d-excess (c).

As altitude increases, vapor $\delta^{18}O$ and $\delta^{2}H$ decrease due to condensation and precipitation processes that occur as air masses ascend, which preferentially remove heavier isotopes following Rayleigh distillation (Dansgaard, 1964). Meanwhile, the d-excess rises. This pattern aligns with previous observations in the lower troposphere (He and Smith, 1999; Salmon et al., 2019) and simulations of complete vertical profiles (Bony et al., 2008).

In our observations, the variation in $\delta^{18}O$ across the vertical profile from ground level at 3856 meters to 11 km is approximately 10-15‰. However, as altitude increases, the air becomes progressively drier, leading to a greater disparity in humidity between the air collected in the air bag and the surface storage environment. This aligns with the variations in Subsection 4.2.2 (Figs. 5b, 5d, and 6b, 6d). The strong kinetic fractionation driven by the diffusion of air into the air bag results in a decrease in the water vapor $\delta^{18}O$ within the bag. After applying model corrections, the corrected $\delta^{18}O$ inside the bag increased slightly compared to pre-correction levels. As described in Subsection 4.2, vapor flux with higher d-excess entering the bag increases the d-excess inside. As a compensation, the diffusion model applies corrections, resulting in a reduced d-excess after correction (Fig. 7c and 10).

4.4 Uncertainty estimates

According to the method of uncertainty estimation elaborated in Subsection 3.4.2, we determined the ranges for four errors to evaluate uncertainty (Table 1).

删除[di wang]: In this dataset, acquired from the drones observations and subsequently corrected using the diffusion modeling, data points with d-excess values less than 1‰ were omitted, as these values are unrealistic and likely result from overcorrection of the δ-values. This resulted in the exclusion of 6 out of 1039 samples.

删除[di wang]: values

删除[di wang]: value

删除[Administrator]: third scenario

删除[di wang]: reduction

删除[di wang]: of

删除[di wang]: values

删除[Administrator]: After applying model corrections, the initial vapor $\delta^{18}O$ inside the air bag were slightly increased.

删除[Administrator]: during storage in the air bag,

删除[Administrator]: in the air bags

删除[di wang]: value

删除[di wang]: source

删除[di wang]: 2

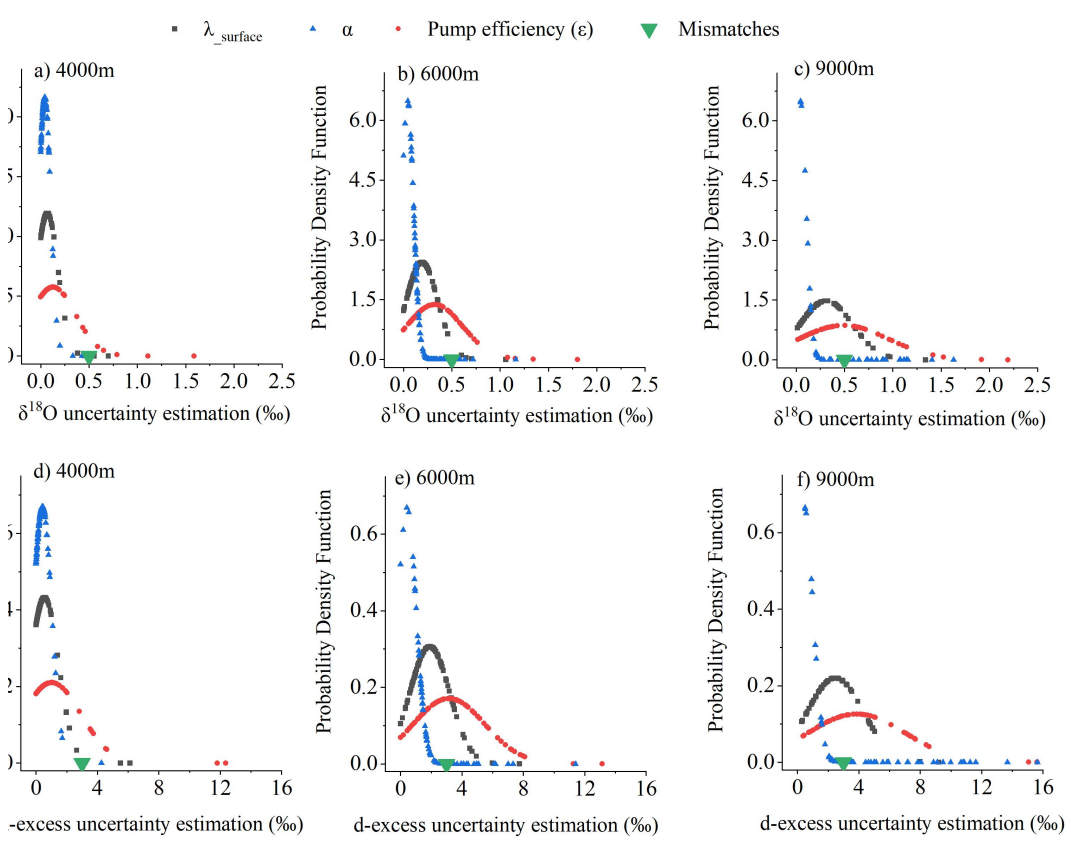

536

537

Figure 8: Contributions of differentsources of uncertainty for $\delta^{18}O$ (a, b, c for 4000m, 6000m, 9000m, respectively) and d-excess (d, e, f for 4000m, 6000m, 9000m, respectively).

删除[di wang]:

The green triangle shows the average mismatch between the model and experimental results.

We analyzed the contributions of uncertainty sources to vertical vapor $\delta^{18}O$ and d-excess measurements at different altitudes using probability density function plots (Fig. 8). The mismatch between the model and the experiment (green marker), calculated using the method described in Subsection 3.4.2, is assumed to remain constant across all altitudes. The other three error sources manifest as unimodal normal distributions at various altitudes for both $\delta^{18}O$ and d-excess. Errors due to uncertainties in pump efficiency (ε) are the main source, exhibiting the largest spread (Fig. 8) and increasing with altitude (Fig. 9). Errors derived from $\lambda_{surface}$ and αalso increase with altitude (Figs. 8 and 9). As a result, at higher elevations, the satellite $\delta^{2}H$ differs more from the measured and corrected data than at lower altitudes (Fig. 10). This pattern arises because λ_{alt} deviates more from $\lambda_{surface}$ at higher elevations (Eq.16), primarily due to increased errors in estimating M_{alt}, amplifying correction errors. Moreover, the humidity and isotopic disparity between the air captured in the air bag and lower-altitude ambient air widens with altitude, requiring more intensive corrections. Consequently, both the uncertainty (Figs. 8 and 9) and the magnitude of the diffusion correction (Fig. 7) increase with altitude.

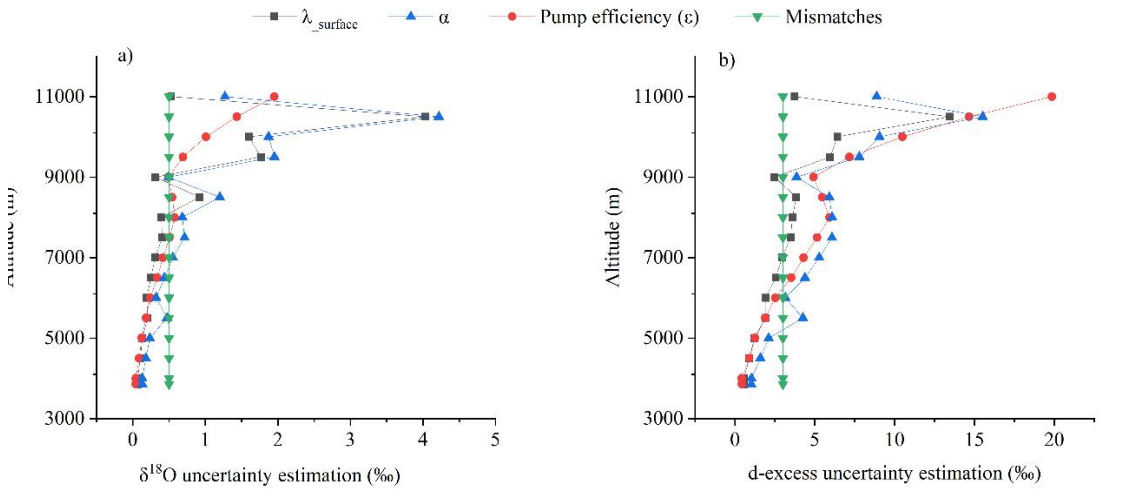

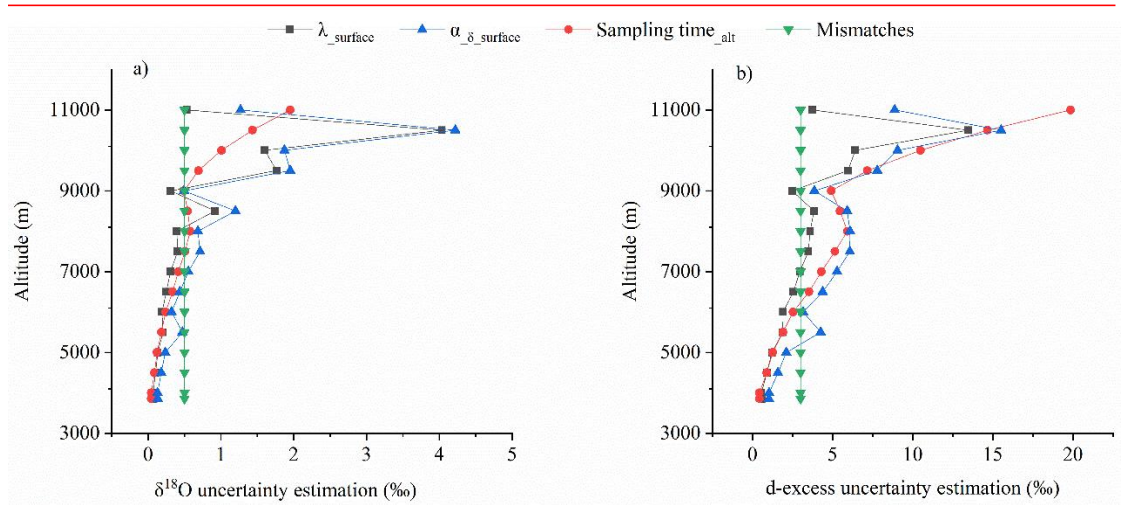

Figure 9 Mean uncertainty of $\delta^{18}O$ (a) and d-excess (b) with altitude for different sources.

On the contrary, errors pertaining to $\lambda_{surface}$ and αdiminish at altitudes exceeding 10,500

删除[di wang]: Sampling time_alt

删除[Administrator]: _δ

删除[di wang]: values

设置格式[di wang]: 缩进: 首行缩进: 0 字符

设置格式[di wang]: 上标

删除[di wang]: emerges because,

设置格式[di wang]: 下标

设置格式[di wang]: 下标

设置格式[di wang]: 字体: 非倾斜

删除[di wang]: estimating λ_{alt} correlated with M based on $\lambda_{surface}$, with M at high altitude derived from the Sampling $time_{alt}$ using Equation 13. This approach can introduce more significant errors at higher altitudes. As altitude increases,

删除[di wang]: conditions

删除[di wang]: Overall, the total error remains within 1‰ for $\delta^{18}O$ and 8‰ for d-excess across 98% of the data.

删除[Administrator]: _δ

meters. This phenomenon may be attributed to our sampling methodology. Although we collected air samples in sequence from low to high altitudes, these samples were measured in reverse order, from high to low altitudes. Consequently, samples taken from the highest altitudes had the shortest storage durations, typically ranging from 10 minutes to two hours. Additionally, we extended the sampling times with increasing altitude (Fig. A1). These extended sampling periods and reduced storage durations help to partially offset the amplified disparities observed between the raw and corrected profiles at higher altitudes. During the drone-based sampling period, which lasted around 10-20 minutes, the external conditions impacting the air bags were not the ground-level environmental values used in the model but rather those of the vertical profile. However, the humidity at higher altitudes is lower than at ground level, and the isotopic composition are closer to those inside the airbag. Consequently, its impact on the airbag's internal conditions is less significant than suggested by using ground-level environmental values. Therefore, the overestimated error in our model accounted for these potential discrepancies.

The combined uncertainty from all sources, including $\lambda_{surface}$, α, pump efficiency (ε), and model-experiment mismatches, results in a total uncertainty of approximately 1‰ for $\delta^{18}O$ and 8‰ for d-excess across 98% of the data. Among these sources, ε contributes the largest uncertainty, particularly at higher altitudes (Fig.8), likely due to the conservative uncertainty range we applied to account for potential reductions in collected air mass at high altitudes. Additionally, $\lambda_{surface}$ and α also contributes considerably to the total uncertainty (Figs. 8 and 9). To mitigate this, we recommend conducting multiple measurements to obtain an averaged value and performing repeated parameter validation to ensure robustness.

删除[di wang]: drone's descent

删除[di wang]: isotopic values

4.5 Comparison with Picarro measurements and satellite data

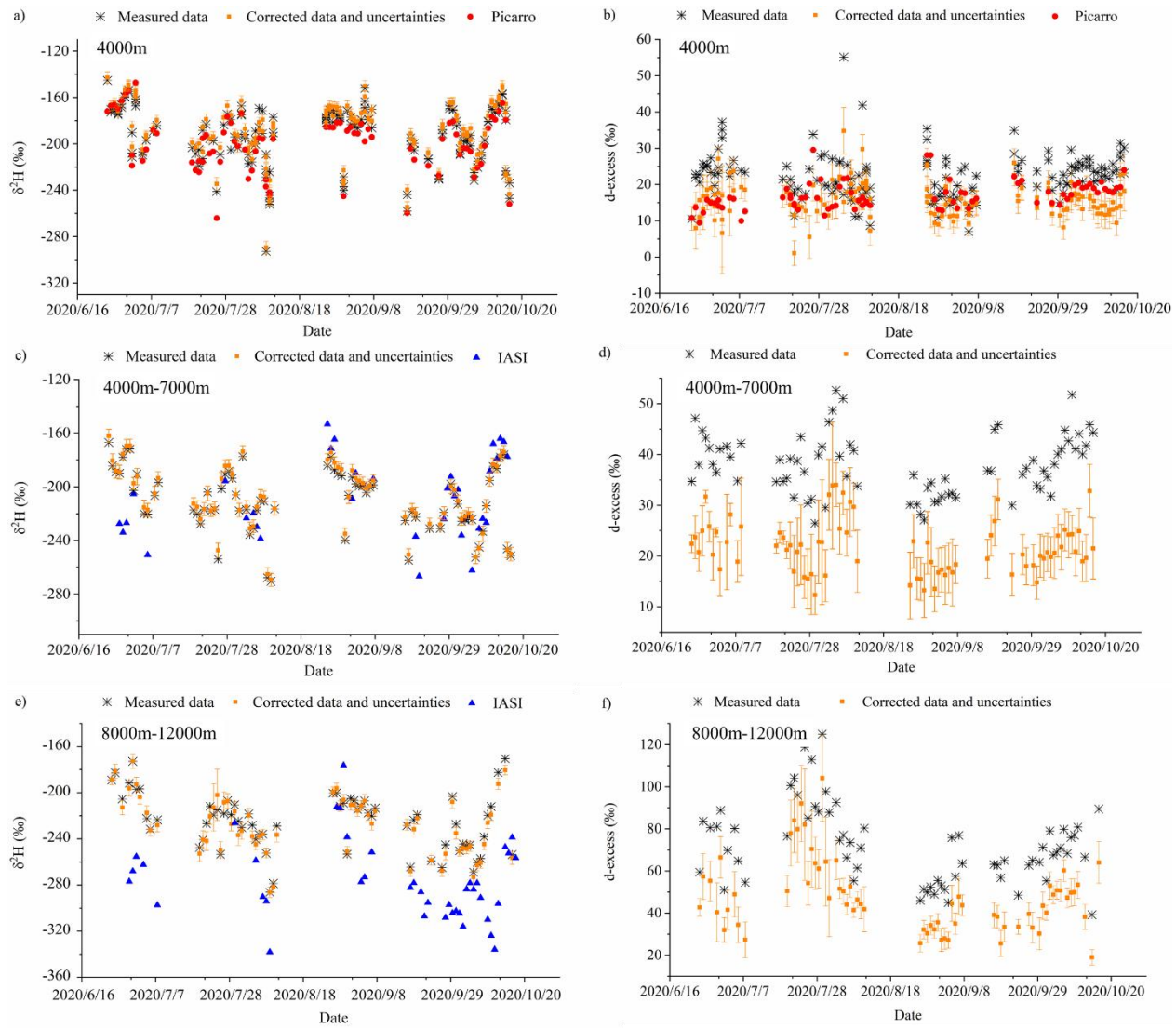

Figure 10 Time series comparison for δ^2H (a, c, e) and d-excess (b, d, f):

(a, b) Raw and corrected (with uncertainties) altitude-averaged air bag measurements from 3856 m to 4000 m, compared with in-situ surface-level measurements at 3856 m taken by the Picarro (legend: Picarro).

(c, d) Raw and corrected (with uncertainties) altitude-averaged air bag measurements from 4000 m to 7000 m, compared with satellite data (IASI).

(e, f) Raw and corrected (with uncertainties) altitude-averaged air bag measurements from 8000 m to 12000 m, compared with satellite data (IASI).

The left panel of Fig.10 (Figs.10 a, c, and e) shows the comparison of raw and corrected water vapor δ^2H measurements at different altitudes with in-situ surface-level measurements on the Picarro , or IASI satellite data at corresponding altitudes. There is notable agreement between the raw measurements and corrected δ^2H for altitudes 3856-4000m and the water vapor δ^2H observed directly by Picarro at ground level (3856m) (Fig.10a). To compare

删除[di wang]: ^{18}O

设置格式[di wang]: 上标

删除[di wang]:

删除[di wang]: *direct Picarro observations*

删除[di wang]: Figure

删除[di wang]: ^{18}O

删除[di wang]: direct Picarro observations

删除[di wang]: ^{18}O

删除[di wang]: ^{18}O

corrected measurements with independent observations at higher altitudes, we refer to the IASI satellite dataset. We acknowledge that this comparison is qualitative, as satellite data represent vertical averages over layers defined by averaging kernels, and therefore differ in measurement footprints (both horizontal and vertical) and spatio-temporal sampling disparities (Shi et al., 2020). Therefore, this comparison remains qualitative. For most intervals, IASI satellite data closely matches raw and corrected δ^2H measurements for altitudes 4000–7000m. In the 8000–12000m range, IASI data is lower than δ^2H observations during certain periods, particularly June and September 2020. While the IASI data closely matches the observed δ^2H for all other periods in the 4000–7000 meter range, it is also lower in June 2020. A more quantitative analysis could be facilitated if an averaging kernel is used to smooth the observed profiles (Herman et al., 2014). All comparisons reflect consistent temporal variations.

The right panel of Fig.10 (Figs.10 b, d, and f) shows the comparison of raw and corrected vapor d-excess measurements. In the 4000m observations (Fig. b), raw d-excess values in air bags were higher than corrected values due to kinetic fractionation during diffusion. After correction, d-excess decrease and are similar to in-situ surface-level measurements on the Picarro at 3856 m. For the 4000–7000m and 8000–12000m observations, no d-excess dataset is available for comparison (Fig. 10d and f). As previously noted, raw d-excess are higher than corrected data due to kinetic fractionation. After correction, d-excess decreases. For the 8000–12000 m observations, the correction magnitude is smaller than at lower altitudes due to the shorter storage time of the air bags.

删除[di wang]: complicated by differences

删除[di wang]: ^{18}O

删除[di wang]: ^{18}O

删除[di wang]: ^{18}O

删除[di wang]: values

删除[di wang]: Figure

删除[di wang]: values

删除[di wang]: surface direct Picarro observations

删除[di wang]: values

5 Conclusion

High spatial and temporal resolution water vapor isotope data are critical for understanding various hydrologic cycle processes. However, observations of vertical water vapor isotope profiles are scarce, particularly in the upper troposphere. Satellite-derived vapor isotope data are available only at limited vertical and temporal resolutions. Acquiring high-resolution water vapor isotope data, especially under conditions where direct measurements are difficult, has been a significant challenge for the water isotopes research community. This study demonstrates the potential of a drone-based air bag sampling method to overcome this challenge and offers solutions for evaluating air bag suitability and addressing air bag permeability.

While air bags offer the advantage of sample collection, their inherent permeability can affect the sealing integrity of the samples, leading to potential contamination. The permeability of airbag materials varies, with some exhibiting lower levels. We recommend prioritizing the use of glass containers and air bags with the lowest permeability for collecting water vapor using portable devices. Additionally, it is essential to conduct the permeability experiments described in this article before any experimental undertaking. This involves storing water vapor with known isotopic composition in the portable collection device for an extended period and then re-measuring these values to assess or determine the device's permeability parameters.

To further address the permeability challenge, we developed a mathematical model to

删除[di wang]: isotopic values

evaluate and correct for diffusion and isotopic fractionation, ensuring the reliability of vapor isotope measurements using air bags. Calibrated with parameters from laboratory experiments, our correction model reconstructs the initial isotopic composition of sampled vapor by using data from both the air bag and the surrounding environment, offers a practical solution to the prevalent permeability challenges. This model was rigorously validated against observational experiments conducted under varying conditions. We also applied this model to drone-collected samples at various pressures. By estimating uncertainty and comparing corrected data with in-situ surface-level measurements on the Picarro and satellite observations, we validated the reliability and applicability of drone-based water vapor isotope measurements.

Our drone-based sampling system, combined with the diffusion model, effectively addresses the limitations of traditional high-altitude water vapor measurement methods. It meets the need for lightweight equipment while providing a more economical, efficient, and flexible alternative to conventional approaches involving large aircraft, airships, and balloons. This approach enables us to exploit the benefits of drone-based air bag sampling at very high altitudes and over long distances, while effectively mitigating its potential limitations. This strategy significantly broadens its potential applications across various environments, thereby enhancing the range and richness of data that can be gathered for water vapor isotope research.This study was conducted under stable temperature and equal internal and external pressures during storage, meaning vapor transport across the bag membrane is driven only by humidity gradients. Our goal was to develop a method for reconstructing the initial isotopic composition of the sampled vapor using measurements from both inside the bag and the surrounding environment under these controlled conditions. We acknowledge that a formulation based on partial pressure of water vapor would be more general and could improve model applicability under varying temperature and pressure conditions. Future work could extend the model to account for these factors in field applications.

删除[di wang]: laser spectroscopy

删除[di wang]: ,

删除[di wang]: meeting

删除[di wang]: and

删除[di wang]: solution for high-altitude water vapor measurements compared to traditional methods

删除[di wang]:

设置格式[di wang]: 缩进: 首行缩进: 2 字符

Appendix A

Table S1 Summary of experiments: diffusion parameter quantification, model validation and differences in experimental methods. $\lambda_{\_surface}$ denotes the water vapor conductance at the surface, α refers to the fractionation coefficient of isotopes, q_0 represents the initial vapor humidity in the air bags, and q_e corresponds to the environmental vapor humidity.

Experiment Number	Experimental purpose	Differences in experimental methods
No. 1	Quantification of $\lambda_{\_surface}$	Dry air in the air bags
No. 2	Quantification of α	Water vapor with known isotopic compositions in the air bags under the condition $q_0 = q_e$
No. 3	Diffusion model validation	Water vapor with varying isotopic compositions and humidity levels in the air bags

删除[di wang]: *diffusion coefficient of humidity*

删除[Administrator]: _δ

删除[Administrator]: _δ

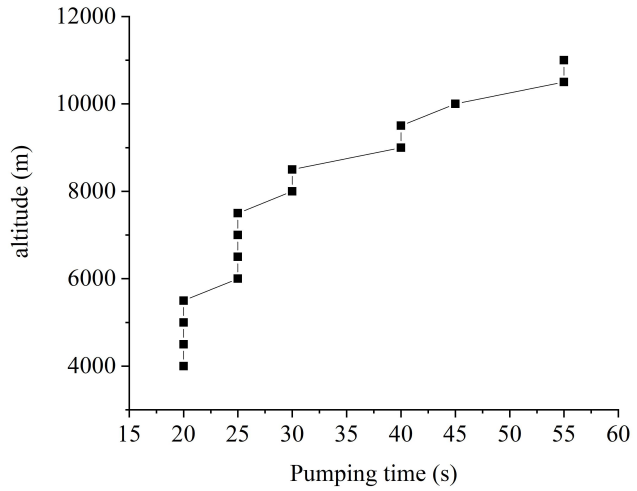

Figure S1 Sampling duration variation with altitude.

删除[di wang]: A1

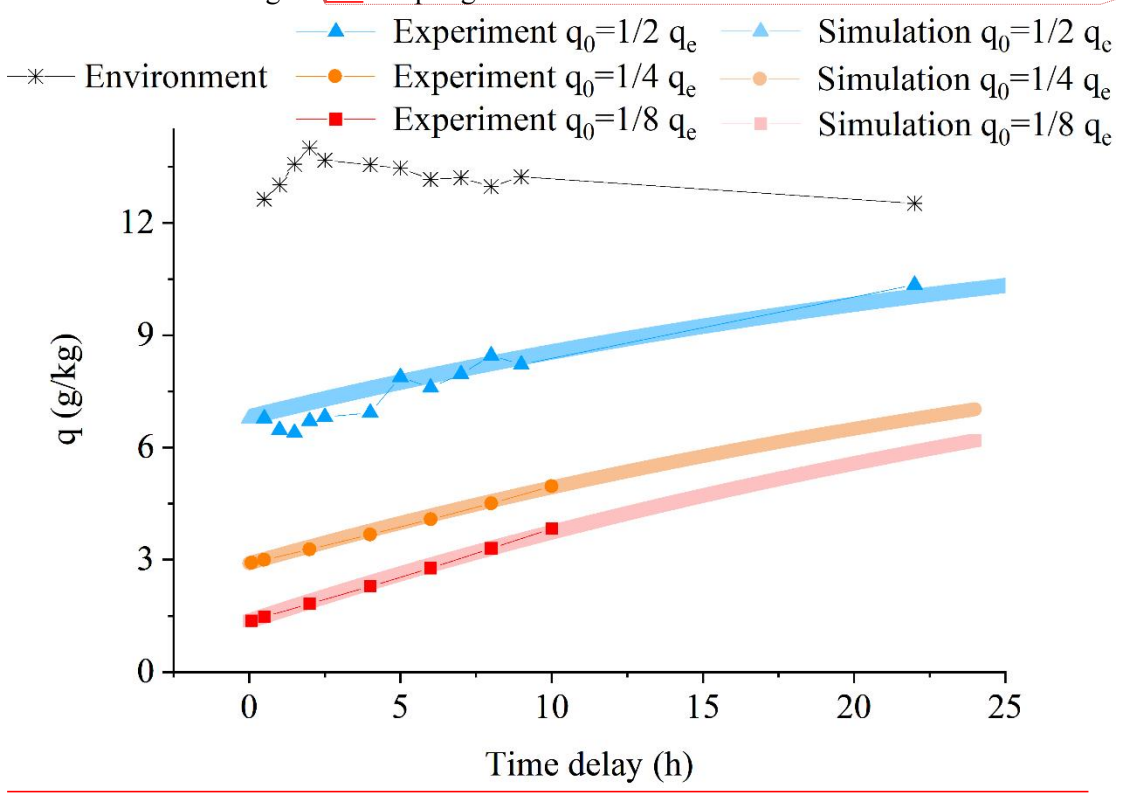

Figure S2 Comparison of humidity variation within the air bag over time in laboratory permeability Experiments No.3 (markers) and diffusion model simulations (lines) for Figures 4 and 5. The experiments cover a range of initial humidities at t = 0 (q_0), from approximately 1/8 * q_e to 1/2 q_e, where q_e denotes environmental humidity.

Code availability

The diffusion modeling code, which simulates the evolution of water vapor isotopes in the airbag and corrects them to their initial values, is available at:
https://github.com/DishiWANG0608/Correcting-for-water-vapor-diffusion.git

Data availability

Data are available from the authors on request.

Video supplement

A video showcasing our field campaign on drone-derived water vapor isotope sampling up to the upper troposphere (11 km) during convective activity, including the workflow for airbag water vapor isotope sampling, is currently available upon request and will be publicly accessible in the near future. Please contact the corresponding author for access (di.wang@latmos.ipsl.fr).

删除[di wang]: lmd

Author contributions

D.W., C.R., and L.T. designed the research, established the subjects of the methodology, and performed the analysis; D.W. and D.Y. conducted the observations; G.B., S.F., H.P. and L.L. contributed to the establishment of methodologies, data calibration, and analysis; Y.S. provided assistance with the computing; All authors contributed to the discussion of the results and the final article; D.W. drafted the manuscript with contributions from all co-authors.

删除[di wang]: J

删除[di wang]: T

Competing interests

The contact author has declared that none of the authors has any competing interests.

Acknowledgments

The authors gratefully acknowledge the Infrared Atmospheric Sounding Interferometer (IASI) for providing spatiotemporal coverage of δ^2H retrieval. We thank Jiaping Xu, Mingjian Chen, Le Chan, and Yao Yao for their irreplaceable help in the development of the drones. We are grateful to the management of 99 Dragon, Mountain Laojun in Lijiang for facilitating the field experiments. We thank Pengbin Liang and Jiangrong Tai for partially participating in the

field observations. We acknowledge Hans Christian Steen-Larsen and Harald Sodemann for their discussions on the correction method. We acknowledge the use of OpenAI's ChatGPT to assist in refining the language. This work was supported by the National Natural Science Foundation of China (Grants No.U2202208 and 42401043), the Strategic Priority Research Program of the Chinese Academy of Sciences (Grant No. XDB40000000), and the Science and Technology Department of Yunnan Province (202201BF070001-021). Di Wang acknowledges support from Chinese Scholarship Council and the Postdoctoral Fellowship Program of CPSF (Grant No. GZC20241440). Siteng Fan acknowledges support from the Marie Skłodowska-Curie Actions of European Research Executive Agency (Grant No. 101064814) and the High Level Special Fund of Southern University of Science and Technology (Grant No. G03050K001).

删除[di wang]: under Grant Number

References

Ayliffe, L., Cerling, T., Robinson, T., West, A., Sponheimer, M., Passey, B., Hammer, J., Roeder, B., Dearing, M., and Ehleringer, J.: Turnover of carbon isotopes in tail hair and breath CO 2 of horses fed an isotopically varied diet, Oecologia, 139, 11-22, 2004.

Bony, S., Risi, C., and Vimeux, F.: Influence of convective processes on the isotopic composition (δ18O and δD) of precipitation and water vapor in the tropics: 1. Radiative-convective equilibrium and Tropical Ocean–Global Atmosphere–Coupled Ocean-Atmosphere Response Experiment (TOGA-COARE) simulations, Journal of Geophysical Research: Atmospheres, 113, 2008.

Bowen, G. J., Cai, Z., Fiorella, R. P., and Putman, A. L.: Isotopes in the Water Cycle: Regional-to Global-Scale Patterns and Applications, Annual Review of Earth and Planetary Sciences, 47, 2019.

Brienen, R. J., Schöngart, J., and Zuidema, P. A.: Tree rings in the tropics: insights into the ecology and climate sensitivity of tropical trees, Tropical tree physiology: adaptations and responses in a changing environment, 2016. 439-461, 2016.

Cerling, T. E., Wittemyer, G., Rasmussen, H. B., Vollrath, F., Cerling, C. E., Robinson, T. J., and Douglas-Hamilton, I.: Stable isotopes in elephant hair document migration patterns and diet changes, Proceedings of the National Academy of Sciences, 103, 371-373, 2006.

Dansgaard, W.: Stable isotopes in precipitation, Tellus, 16, 436-468, 1964.

Diekmann, C. J., Schneider, M., Ertl, B., Hase, F., García, O., Khosrawi, F., Sepúlveda, E., Knippertz, P., and Braesicke, P.: The global and multi-annual MUSICA IASI {H2O, δD} pair dataset, Earth Syst. Sci. Data, 13(11), 5273–5292, 2021.

Galewsky, J., Steen-Larsen, H. C., Field, R. D., Worden, J., Risi, C., and Schneider, M.: Stable isotopes in atmospheric water vapor and applications to the hydrologic cycle, Reviews of Geophysics, 54, 2016.

Gat, J. R.: Oxygen and hydrogen isotopes in the hydrologic cycle, Annual Review of Earth and Planetary Sciences, 24, 225-262, 1996.

Ghosh, P. and Brand, W. A.: Stable isotope ratio mass spectrometry in global climate change research, International Journal of Mass Spectrometry, 228, 1-33, 2003.

Gralher, B., Herbstritt, B., and Weiler, M.: Unresolved aspects of the direct vapor equilibration method for stable isotope analysis (δ 18 O, δ 2 H) of matrix-bound water: unifying protocols through empirical and mathematical scrutiny, Hydrology and Earth System Sciences, 25, 5219-5235, 2021.

Grootes, P. M. and Stuiver, M.: Oxygen 18/16 variability in Greenland snow and ice with 10(-3)- to 10(5)-year time resolution, Journal of Geophysical Research-Oceans, 102, 26455-26470, 1997.

He, H. and Smith, R. B.: Stable isotope composition of water vapor in the atmospheric boundary layer above the forests of New England, Journal of Geophysical Research Atmospheres, 104, 11657-11673, 1999.

Hendry, M., Schmeling, E., Wassenaar, L., Barbour, S., and Pratt, D.: Determining the stable isotope composition of pore water from saturated and unsaturated zone core: improvements to the direct vapour equilibration laser spectrometry method, Hydrology and Earth System Sciences, 19, 4427-4440, 2015.

Herbstritt, B., Gralher, B., Seeger, S., Rinderer, M., and Weiler, M.: Discrete in situ vapor sampling for subsequent lab-based water stable isotope analysis, Hydrology and Earth System Sciences, 27, 3701-3718, 2023.

Herman, R., Cherry, J., Young, J., Welker, J., Noone, D., Kulawik, S., and Worden, J.: Aircraft validation of Aura Tropospheric Emission Spectrometer retrievals of HDO/H 2 O, Atmospheric Measurement Techniques, 7, 3127-3138, 2014.

Hodges, J. T. and Lisak, D.: Frequency-stabilized cavity ring-down spectrometer for high-sensitivity measurements of water vapor concentration, Applied Physics B, 85, 375-382, 2006.

Jiménez-Rodríguez, C. D., Coenders-Gerrits, M., Bogaard, T., Vatiero, E., and Savenije, H.: comparison of water vapor sampling techniques for stable isotope analysis, Hydrology and Earth System Sciences Discussions, 2019. 1-15, 2019.

Johnson, L., Sharp, Z., Galewsky, J., Strong, M., Van Pelt, A., Dong, F., and Noone, D.: Hydrogen isotope correction for laser instrument measurement bias at low water vapor concentration using conventional isotope analyses: application to measurements from Mauna Loa Observatory, Hawaii, Rapid Communications in Mass Spectrometry, 25, 608-616, 2011.

Lacour, J.-L., Risi, C., Clarisse, L., Bony, S., Hurtmans, D., Clerbaux, C., and Coheur, P.-F.: Mid-tropospheric δD observations from IASI/MetOp at high spatial and temporal resolution, Atmospheric chemistry and physics, 12, 10817-10832, 2012.

Lacour, J.-L., Risi, C., Worden, J., Clerbaux, C., and Coheur, P.-F.: Importance of depth and intensity of convection on the isotopic composition of water vapor as seen from IASI and TES δD observations, Earth and planetary science letters, 481, 387-394, 2018.

Michener, R. and Lajtha, K.: Stable isotopes in ecology and environmental science, John Wiley & Sons, 2008.

Millar, C., Pratt, D., Schneider, D. J., and McDonnell, J. J.: A comparison of extraction systems for plant water stable isotope analysis, Rapid Communications in Mass Spectrometry, 32, 1031-1044, 2018.

Muccio, Z. and Jackson, G. P.: Isotope ratio mass spectrometry, Analyst, 134, 213-222, 2009.

Rodgers, C. D. and Connor, B. J.: Intercomparison of remote sounding instruments, Journal of Geophysical Research: Atmospheres, 108, 2003.

Rozmiarek, K. S., Vaughn, B. H., Jones, T. R., Morris, V., Skorski, W. B., Hughes, A. G., Elston, J., Wahl, S., Faber, A.-K., and Steen-Larsen, H. C.: An unmanned aerial vehicle sampling platform for atmospheric water vapor isotopes in polar environments, Atmospheric Measurement Techniques, 14, 7045-7067, 2021.

Salmon, O. E., Welp, L. R., Baldwin, M. E., Hajny, K. D., Stirm, B. H., and Shepson, P. B.: Vertical profile observations of water vapor deuterium excess in the lower troposphere, Atmospheric

Chemistry and Physics, 19, 11525-11543, 2019.

Shi, X., Risi, C., Pu, T., Lacour, J. l., Kong, Y., Wang, K., He, Y., and Xia, D.: Variability of isotope composition of precipitation in the southeastern Tibetan Plateau from the synoptic to seasonal time scale, Journal of Geophysical Research: Atmospheres, 125, e2019JD031751, 2020.

Sprenger, M., Herbstritt, B., and Weiler, M.: Established methods and new opportunities for pore water stable isotope analysis, Hydrological Processes, 29, 5174-5192, 2015.

Steen-Larsen, H. C., Masson-Delmotte, V., Sjolte, J., Johnsen, S. J., Vinther, B. M., Bréon, F. M., Clausen, H. B., Dahl-Jensen, D., Falourd, S., and Fettweis, X.: Understanding the climatic signal in the water stable isotope records from the NEEM shallow firn/ice cores in northwest Greenland, Journal of Geophysical Research Atmospheres, 116, 161-165, 2011.

Wassenaar, L., Hendry, M., Chostner, V., and Lis, G.: High resolution pore water δ2H and δ18O measurements by H2O (liquid)− H2O (vapor) equilibration laser spectroscopy, Environmental science & technology, 42, 9262-9267, 2008.

West, A. G., Goldsmith, G. R., Brooks, P. D., and Dawson, T. E.: Discrepancies between isotope ratio infrared spectroscopy and isotope ratio mass spectrometry for the stable isotope analysis of plant and soil waters, Rapid Communications in Mass Spectrometry, 24, 1948-1954, 2010.

West, J. B., Bowen, G. J., Dawson, T. E., and Tu, K. P.: Isoscapes: understanding movement, pattern, and process on Earth through isotope mapping, Springer, 2009.

Worden, J., Bowman, K., Noone, D., Beer, R., Clough, S., Eldering, A., Fisher, B., Goldman, A., Gunson, M., Herman, R., Kulawik, S. S., Lampel, M., Luo, M., Osterman, G., Rinsland, C., Rodgers, C., Sander, S., Shephard, M., and Worden, H.: Tropospheric emission spectrometer observations of the tropospheric HDO/H2O ratio: Estimation approach and characterization, Journal of Geophysical Research-Atmospheres, 111, 2006.

Yu, W., Tian, L., Ma, Y., Xu, B., and Qu, D.: Simultaneous monitoring of stable oxygen isotope composition in water vapour and precipitation over the central Tibetan Plateau, Atmospheric Chemistry and Physics, 15, 10251-10262, 2015.

设置格式[di wang]: 字体: （默认）Times New Roman